Universiteit Utrecht

Azimuthal angular correlations of heavy flavour decay electrons and charged hadrons in proton-proton collisions at $\sqrt{s}$ = 7 TeV using the ALICE detector

Jasper van der Maarel

July 27, 2013

Master Thesis
Report number: UU(SAP) 13-11

Supervisors:
Dr. André Mischke
Deepa Thomas

Utrecht University
Faculty of Science/Department of Physics and Astronomy
Institute for Subatomic Physics
Buys Ballot laboratory
PO BOX 80 000, 3508 TA Utrecht, The Netherlands

Abstract

Using measurements of the ALICE detector of proton-proton collisions at a center-of-mass energy of $\sqrt{s} = 7$ TeV, the azimuthal angular correlation per trigger between electrons from semi-leptonic decay of heavy flavour mesons and charged hadrons is calculated.

By using Monte Carlo simulations to calculate the correlation distributions for electrons from D and B mesons, the relative beauty contribution to the heavy flavour electron decay spectra was measured. This measurement is compared to earlier performed measurements with the same method in proton-proton collisions at $\sqrt{s} = 2.76$ TeV and measurements with the impact parameter method at $\sqrt{s} = 7$ TeV. The results are in agreement with each other within the statistical and systematic errors. The measured values are also compared to FONLL calculations. An agreement within the uncertainties is found.

The near-side correlation strength was extracted by fitting a Gaussian on the near-side. This was then compared to central and semi-central Pb-Pb collisions at center-of-mass energy per nucleon pair of $\sqrt{s_{\mathrm{NN}}} = 2.76$ TeV. The I_{AA} is the ratio of the yield of Pb-Pb and pp, and is measured to be around 1. This would mean that there is no suppression or enhancement in Pb-Pb collisions. But because of the large uncertainties in the Pb-Pb analysis it is hard to make strong statements about the modification of the yield in the QCD medium.

Contents

1 Introduction

The currently accepted model describing particles and their interactions is called the Standard Model (SM). This model describes three of the four fundamental forces of nature, namely electromagnetism, the weak interaction and the strong interaction. The fourth fundamental force is gravity.

The fundamental particles of the Standard Model are quarks and leptons, which are fermions. Fermions are particles with a half-integer spin. Figure 1 shows the fundamental particles and some of their properties.

Both the quarks and leptons are divided in three families. The quark families each consist of two quarks types (called flavours), one with an electric charge of 2/3 and one with charge -1/3. In order of increasing mass, the positively charged quarks are up (u), charm (c) and top (t). The corresponding negatively charged quarks are down (d), strange (s) and bottom/beauty (b). The lepton families each consist of a lepton type and a corresponding neutrino: electron (e) and electron neutrino (ν_e), muon (μ) and muon neutrino (ν_μ) and tau (τ) and tau neutrino (ν_τ). Each of these particles also have an anti-particle with the same mass and opposite charge. Everyday matter consists of protons and neutrons, which both consist of the two lightest quarks: u and d. Particles that contain heavier quarks are unstable and decay to matter containing only u and d quarks.

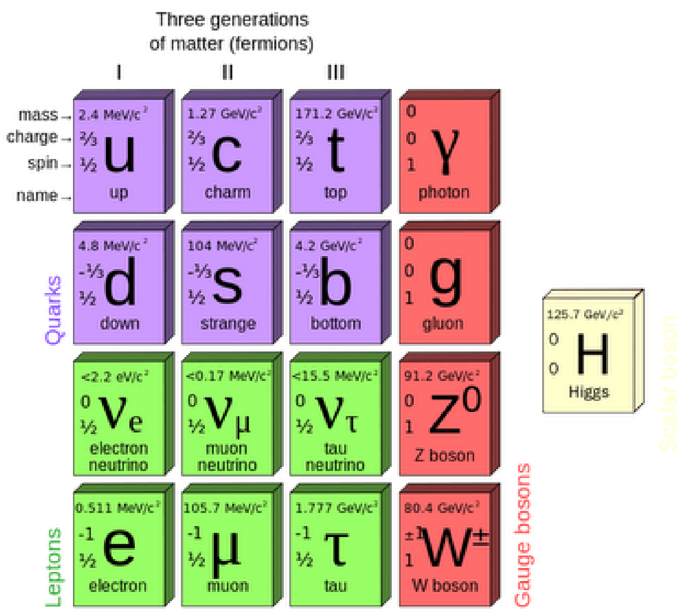

Figure 1: The fundamental particles in the Standard Model.

Interactions between particles arise from the exchange of particles called force carriers, which are bosons. Bosons are particles with integer spin. All charged particles interact via the electromagnetic force, which is mediated by the photon (γ). Neutral particles do not experience this force. The only force that is experienced by all particles is the weak force, mediated by the charged $W^{\pm}$ bosons and neutral Z^0 boson. Quarks additionally interact via the strong force, which has the gluons (g) as force carrier.

Lastly, the Standard Model also requires another massive boson called the Higgs boson. It is responsible for giving mass to other particles via the Higgs mechanism. Recently both ATLAS and CMS reported the discovery of a new particle that is most likely the Higgs boson [1] [2].

1.1 Quantum Chromo Dynamics

The theory describing the strong interaction between quarks and gluons (together called partons) is called Quantum Chromo Dynamics (QCD). In the same way the electromagnetic force has electric charge, the strong force has a charge called colour charge. The charges are red, green and blue. Anti-particles carry an anti-colour (anti-red, anti-green and anti-blue). Unlike the electromagnetic force, where the force carriers (photons) do not have a charge, the force carriers of the strong force (gluons) do have a colour charge. This causes the gluon to both interact with quarks and other gluons.

The coupling constant of a force is a measure for its strength. The coupling constant of the strong interaction α_s becomes stronger when the distance between the colour objects increases, or equivalently for decreasing momentum transfer:

$$\alpha_s(|Q^2|) = \frac{12\pi}{(11n - 2f)\ln(|Q^2|/\Lambda^2)} \quad . \tag{1}$$

Here $|Q^2|$ is the square of the exchanged four-momentum, n the number of colours (equal to 3), f the number of quark flavours (equal to 6) and Λ an experimentally determined constant of about 300 MeV/c.

This dependence of the coupling constant on $|Q^2|$ has two direct consequences: *asymptotic freedom* and *confinement*. Both phenomena will be described below.

1.1.1 Confinement

Confinement implies that quarks can not be observed freely. Instead, they are confined in particles we call hadrons. Attempting to separate the quarks of a hadron will simply create a new quark-antiquark pair when the energy threshold is reached. Hadrons are always colour neutral and consist of two quarks (mesons) or three quarks (baryons). Because of the requirement of colour neutrality, mesons always consist of a quark and an anti-quark of the same colour and baryons consist of quarks with three different colours.

Although the statement that baryons consist of three quarks is enough to form an intuitive picture, it is not entirely correct. Experimental measurements have shown that the three quarks of a proton (uud) only account for roughly half of the momentum of the proton. The rest of the momentum is carried by gluons. Gluons can produce quark-antiquark pairs, therefore there is always a finite chance that the proton contains extra pairs of quarks. These "extra quarks" are called sea quarks, while the three quarks that are always present are called the valence quarks.

1.1.2 Asymptotic freedom

Asymptotic freedom is the phenomenon that at small distances and high energies particles essentially behave like free particles. If one can create a system with sufficiently high energy density, the confinement can not be maintained and a state of matter of deconfined partons is created: the Quark Gluon Plasma.

1.2 Quark Gluon Plasma

Figure 2 shows the phase diagram of strongly interacting matter. In the bottom left corner, corresponding to low density and low temperature, the matter is confined in hadrons. However when the density exceeds 0.7 GeV/fm^3 and temperature exceeds about 175 MeV, a Quark Gluon Plasma (QGP) is formed. Cosmological models predict that the universe was in a state of QGP between 10^{-12} and 10^{-6} seconds after the big bang. For this reason, the study of the properties of the QGP helps to obtain a better understanding of the origin of our universe.

Heavy-ion collisions in particle accelerators provide a way to study the QGP under controlled conditions. The Relativistic Heavy Ion Collider (RHIC) at the Brookhaven National Laboratory collided Au ions with a center of mass energy per nucleon pair of $\sqrt{s_{\mathrm{NN}}} = 200$ GeV and studied the properties of the QGP. However since 2010 the Large Hadron Collider (LHC) at CERN has been colliding lead ions with a center of mass energy of $\sqrt{s_{\mathrm{NN}}} = 2.76$ TeV. In the coming years the energy will be increased to $\sqrt{s_{\mathrm{NN}}} = 5.5$ TeV.

Heavier quarks are formed at an earlier stage in the collision. The three heaviest quarks are in order of decreasing mass the top, beauty and charm quark. The formation time for charm quarks is around 0.1 fm/c and for beauty quarks around 0.02 fm/c. At the energy of the LHC the expected lifetime of the formed QGP is in the order of 10 fm/c. This makes the heavy quarks an important probe for the QGP, since they experience the full evolution of the system. They travel through the medium and lose energy due to gluon radiation and multiple collisions.

In the absence of a QGP, one could describe the collision of heavy ions as a superposition of proton-proton collisions. Any deviation from this behaviour provides information about the QGP. This makes proton-proton collisions an important baseline for studies in heavy ion collisions.

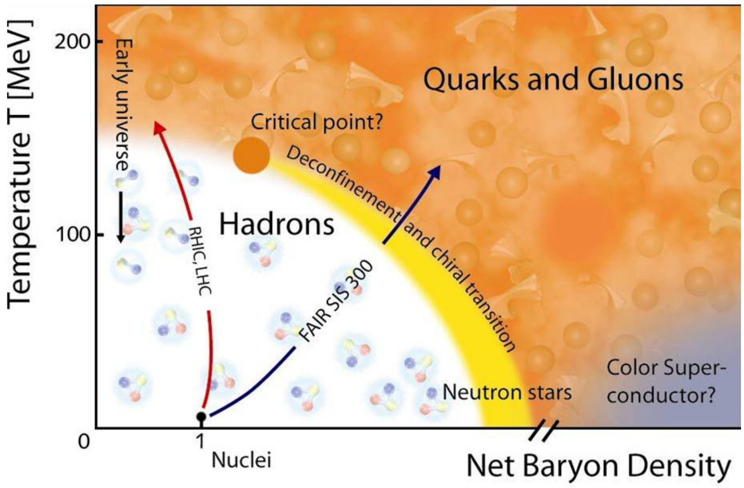

Figure 2: Phase diagram of strongly interacting matter.

1.3 Heavy flavour production

The production of heavy flavour (c and b) in collisions can be predicted using perturbative QCD calculations. However non-perturbative phenomena have an important contribution to these processes. The available calculations that incorporate these non-perturbative effects make use of FONLL (First Order Next to Leading Logarithm) [3]. Next to forming a baseline measurement, proton-proton collisions also form a good tool to test the accuracy of these FONLL calculations.

The produced quarks go through a process called hadronization, in which the quarks combine to form hadrons. Two of the possible mesons that are created are the D and B mesons. They both consist of a heavy (charm or beauty) quark and a lighter quark. These mesons are not stable and eventually decay to other hadrons and leptons, which can be detected.

1.4 Two-particle correlations

By measuring the two-particle correlation of the decay products of the D and B mesons and the hadrons in the event, one could study multiple properties of the QGP medium. Due to the production of heavy flavour quarks always being in pairs (quark anti-quark), the correlation distribution shows two peaks, a near-side peak at $\Delta\varphi = 0$ and an away-side peak at π. Such correlations have been measured with the STAR detector at the RHIC [4]. Figure 3 shows the measured correlation distributions for both proton-proton and gold-gold collisions [4]. The suppression of the away-side peak in Au-Au collisions is one of the first experimental evidence of the QGP. This is because the quark on the away-side travels through the medium and loses energy so it can not escape on the other side.

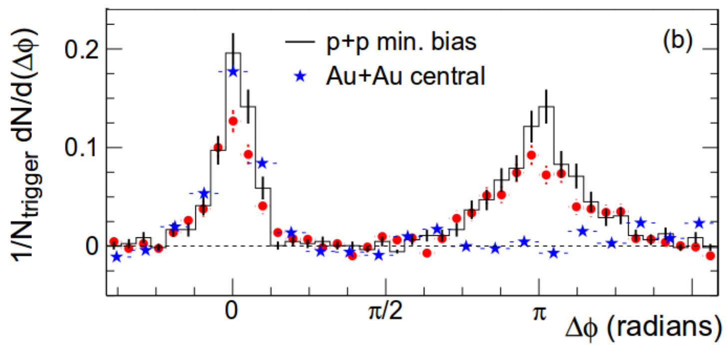

Figure 3: Azimuthal angular correlation distribution for pp and Au-Au collisions [4].

The analysis that is performed by the author and is discussed in this thesis focuses on the correlation between electrons from semi-leptonic decay of D and B mesons and hadrons in proton-proton collisions with a center-of-mass energy of $\sqrt{s} = 7$ TeV. From these correlation distributions two observables are extracted, that will be explained in more detail below:

- The relative contribution of beauty to the heavy flavour electron decay spectrum. This allows to test FONLL predictions.
- A baseline measurement for Pb-Pb collisions. This helps better understand the QGP medium.

1.4.1 Relative beauty fraction

The relative contribution of beauty to the heavy flavour electron decay spectrum (r_{B}) is defined as

$$r_{\mathrm{B}} = \frac{\frac{\mathrm{d}\sigma(\mathrm{B}\to\mathrm{e})}{\mathrm{d}p_{\mathrm{T}}}}{\frac{\mathrm{d}\sigma(\mathrm{B}\to\mathrm{e})}{\mathrm{d}p_{\mathrm{T}}} + \frac{\mathrm{d}\sigma(\mathrm{D}\to\mathrm{e})}{\mathrm{d}p_{\mathrm{T}}}} \quad . \tag{2}$$

Here $\mathrm{d}\sigma/\mathrm{d}p_{\mathrm{T}}$ is the differential cross section for that particular process. The D mesons either come directly from the charm (this is called prompt D) or come from the decay of a B meson: $\mathrm{B} \to \mathrm{D} \to \mathrm{e}$. This is called B feed down, and this contribution needs to be added to the B:

$$r_{\mathrm{B}} = \frac{\frac{\mathrm{d}\sigma(\mathrm{B}\to\mathrm{e})}{\mathrm{d}p_{\mathrm{T}}} + \frac{\mathrm{d}\sigma(\mathrm{B}\to\mathrm{D}\to\mathrm{e})}{\mathrm{d}p_{\mathrm{T}}}}{\frac{\mathrm{d}\sigma(\mathrm{B}\to\mathrm{e})}{\mathrm{d}p_{\mathrm{T}}} + \frac{\mathrm{d}\sigma(\mathrm{B}\to\mathrm{D}\to\mathrm{e})}{\mathrm{d}p_{\mathrm{T}}} + \frac{\mathrm{d}\sigma(\mathrm{D}\to\mathrm{e})}{\mathrm{d}p_{\mathrm{T}}}} \quad . \tag{3}$$

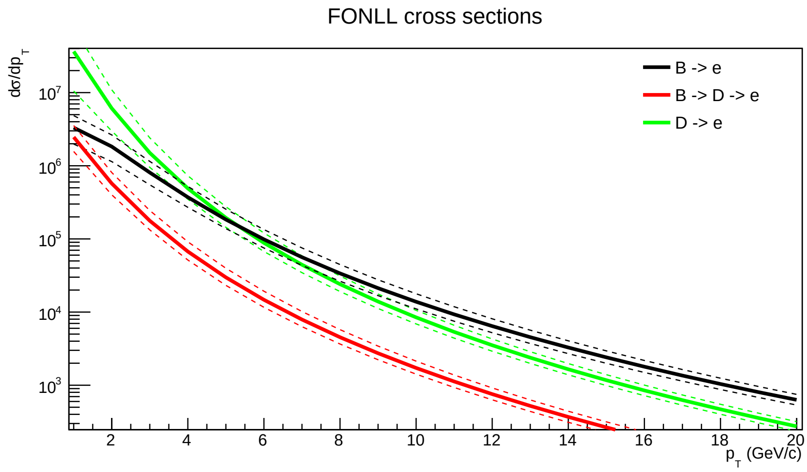

Figure 4: FONLL predictions for the differential cross sections [5].

FONLL predicts values of all three differential cross sections as function of the transverse momentum [5], as is shown in Figure 4. Using (3) the relative beauty fraction can be calculated. Using electron-hadron correlations, the r_{B} as function of p_{T} can be measured. The method of extracting this will be explained in Section 5. The measurement can then be compared to the FONLL prediction.

1.4.2 Baseline measurement

The I_{AA} is the ratio of the correlation strengths in Pb-Pb and pp. Here pp collisions form a baseline measurement. The I_{AA} could tell us about a possible enhancement or suppression in lead-lead compared to proton-proton. In this analysis we look at the yield on the near-side, which might tell us more about the hadronization in lead-lead collisions, if it happens in the QGP medium or outside.

Measurements of hadron-hadron correlations show a near-side enhancement of I_{AA} [6]. The I_{AA} is sensitive to:

1. A change of the fragmentation function. If the fragmentation function is softened in the medium, hadrons carry a smaller fraction of the initial parton momentum in Pb-Pb collisions as compared to pp collisions. Therefore, hadrons with a given p_{T} originate from a larger average parton momentum which may lead to more associated particles, and thus $I_{\mathrm{AA}} > 1$.
2. A change of the quark/gluon jet ratio in the final state due to the different coupling to the medium. More gluon jets lead to a similar effect to softening of the fragmentation function and results in $I_{\mathrm{AA}} > 1$.

3. A bias on the parton p_{T} spectrum after energy loss due to the trigger particle selection. A different parton distribution in pp and Pb-Pb collisions can modify the I_{AA} even if fragmentation of a given parton after energy loss is unmodified. The yield of trigger particles is quantified by the R_{AA}, the ratio of the yield of trigger particles in Pb-Pb and pp collisions, divided by the number of binary collisions. Measurements have shown that that the R_{AA} is strongly suppressed with a rising slope as function of p_{T}. A similar suppression should also apply to the partons. This means that the parton distribution is biased towards the high p_{T}, which leads to a higher I_{AA}.

It is likely that all of these effects play a role. Measuring both R_{AA} as well as I_{AA} might give insight in the interplay of energy loss and the change of the fragmentation in the medium.

2 Experimental setup

This section describes the complete experimental setup. First the accelerator is described, next the detector and the specific parts of the detector that were used for the analysis and finally the computer framework that was used to analyse the data.

2.1 Large Hadron collider

The Large Hadron Collider (LHC) is the largest accelerator at CERN and is currently the most powerful accelerator in the world. The accelerator lies in a 26.7 km long tunnel underground across the border between France and Switzerland. The LHC is designed to collide protons with a center-of-mass energy of up to $\sqrt{s} = 14$ TeV and lead ions with a center-of-mass energy per nucleon pair of up to $\sqrt{s_{\rm NN}} = 5.5$ TeV. The currently reached energies are $\sqrt{s} = 7$ TeV for proton-proton collisions and $\sqrt{s_{\rm NN}} = 2.76$ TeV for lead-lead collisions.

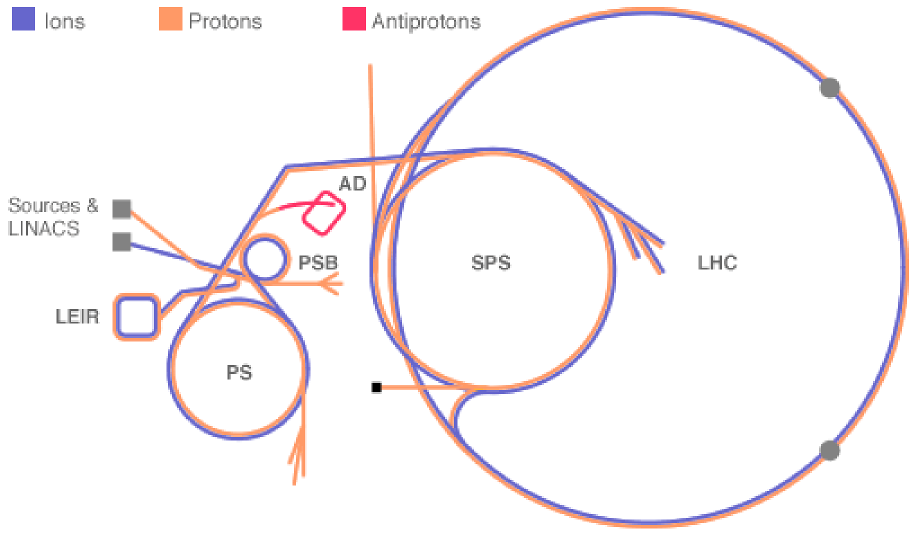

Figure 5: Schematic view of the accelerator complex at CERN.

Figure 5 shows a schematic of the accelerators at CERN. Before particles are injected in the LHC they are already accelerated by several beam lines. The particles are extracted from a source, which is a hydrogen tank for protons and a piece of isotopically enriched lead for the heavy ion collisions, and first injected into the Linear Accelerator 2 (Linac2). From this they go through the Proton Synchrotron Booster (PSB), the Proton Synchrotron (PS) and the Super Proton Synchrotron (SPS). At each step they acquire a higher energy. After the SPS the particles have an energy of 450 GeV and are injected into the LHC where they are further accelerated.

The LHC tunnel contains two beam pipes that intersect at multiple points. At four of these points there are detectors placed that detect the collisions. The four detectors are ALICE, ATLAS, CMS and LHCb.

2.2 A Large Ion Collider Experiment

A Large Ion Collider Experiment (ALICE) is a heavy-ion experiment with the main goal of exploring the characteristics of the strong interacting medium produced in the heavy ion collisions. ALICE is capable of tracking charged particles in a wide transverse momentum range and has excellent particle identification capabilities [7].

Figure 6 shows a schematic view of the detector. The detector is divided in two regions: a central barrel centered around the interaction point and a forward part.

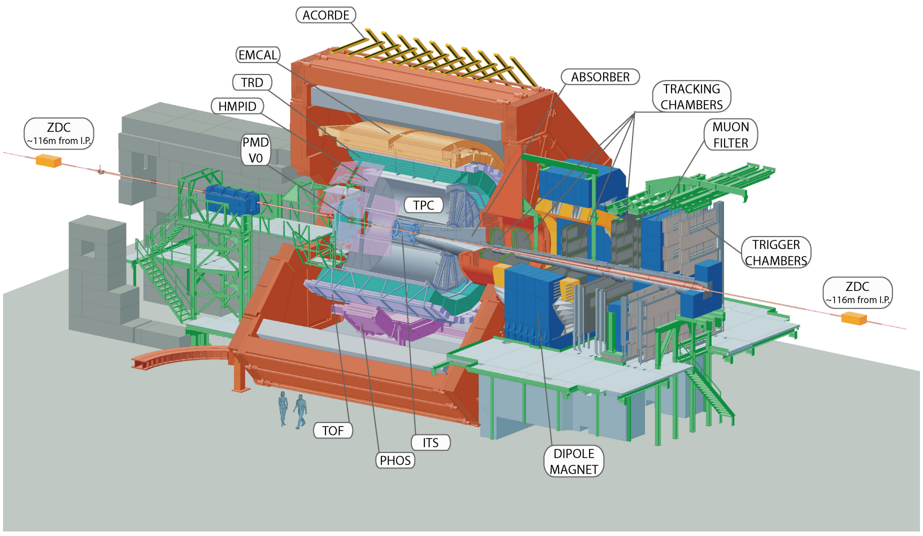

Figure 6: Schematic view of the ALICE detector.

The detectors of the central barrel are installed inside a solenoid that can create a 0.5 T magnetic field. From the inside out the central barrel contains: the Inner Tracking System (ITS), the Time Projection Chamber (TPC), Transition Radiation Detector (TRD) and Time Of Flight Detector (TOF). These detectors cover the full azimuthal range and cover $|\eta| < 0.9$. There are also two detectors that cover a smaller range, which are the High Momentum Particle Identification Detector (HMPID) and the Electromagnetic Calorimeter (EMCal).

The forward part consist of muon trackers, multiplicity detectors (Photon Multiplicity Detector and Forward Multiplicity Detector), Zero Degree Calorimeters

(ZDC) and the trigger detectors VZERO and T0.

Below we will discuss all the subdetectors that are relevant for the performed analysis.

2.2.1 Inner Tracking System

The Inner Tracking System (ITS) is the detector closest to the interaction point. It consists of six cylindrical layers of silicon detectors with a radius between 3.9 cm and 43.0 cm. The first two layers, located at 3.9 cm and 7.6 cm are made of Silicon Pixel Detectors (SPD). The distance between the beam pipe and the first layer is 0.9 cm. The next two layers are made of Silicon Drift Detectors (SDD) and are located at radii of 15 cm and 23.9 cm. The two outer layers are located at 38.0 cm and 43.0 cm and are made of Silicon Strip Detectors (SSD). The Silicon Strip Detectors are built at the Utrecht University.

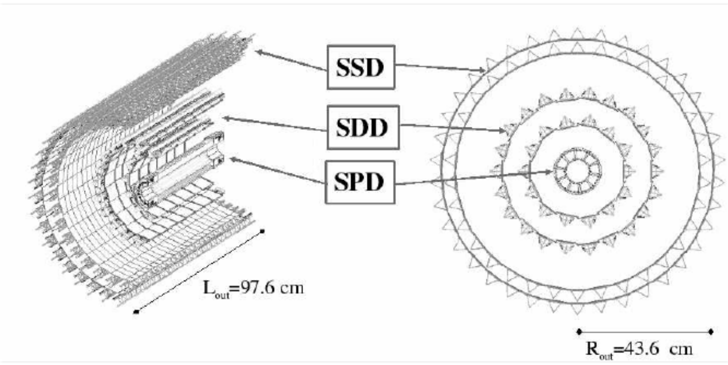

Figure 7: Layout of the Inner Tracking System.

The primary use of the ITS is identifying the primary and secondary vertex. It is also used to detect low momentum particles and improve the momentum resolution in general.

Because the first two layers are the closest to the interaction point, the particle density will be higher compared to the other layers (up to 80 particles per cm^2 in the SPD and < 1 particle per cm^2 in the SSD). This is why the first two layers are made of pixel detectors. These have the largest spatial precision in $r\varphi$: 12 μm compared to 38 μm and 20 μm in the SDD and SSD, respectively. The spatial precision in the z direction is 100 μm for the SPD, 28 μm for the SDD and 830 μm for the SSD. The outer layers have a lower resolution because the particle density will be much less lower.

2.3 Time Projection Chamber

The TPC is the main tracking device in the ALICE detector. Figure 8 shows the layout of the TPC. It is a 510 cm long gas chamber. The gas gets ionized when a charged particle passes through, allowing tracking of the particle. The main uses for the TPC are: tracking, momentum measurements with a good track separation and energy loss ($\mathrm{d}E/\mathrm{d}x$) measurements.

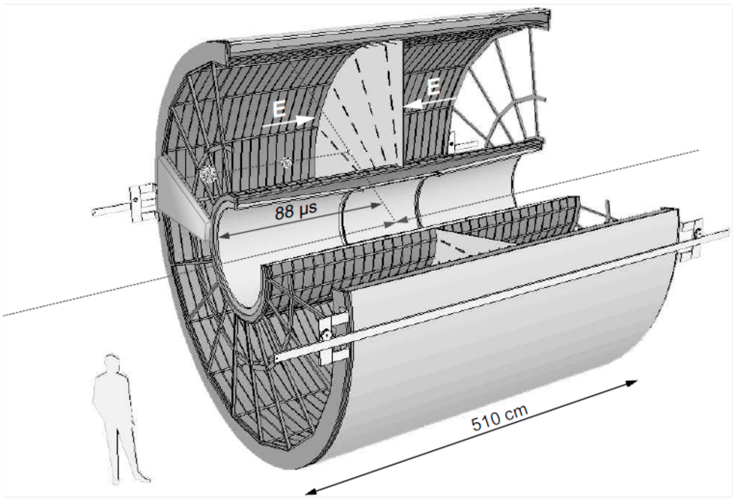

Figure 8: Layout of the Time Projection Chamber.

2.4 Electromagnetic Calorimeter

The Electromagnetic Calorimeter (EMCal) is a calorimeter [8], which means that it measures the energy of particles. This is done by towers of Pb scintillators. Two by two towers form a module, which are assembled in strip modules of 12 modules each. These strip modules are then grouped in super modules. The EMCal contains 12,288 towers in total. Figure 9 shows the layout of the EMCal detector, mounted on its support structure. It covers an area of 107° in the φ direction and has an acceptance of $|\eta| < 0.7$ and is located about 4.5 m from the beams in the radial direction.

The EMCal provides energy measurement of charged particles that travel through it. But it also acts as a trigger for photons and electrons. This means that the event is only recorded if the EMCal detect a particle with an energy above the threshold. This allows us to obtain a higher momentum range than without this trigger.

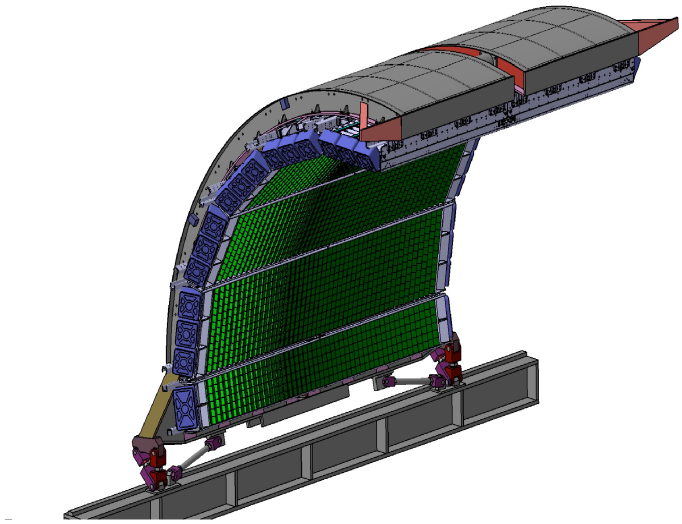

Figure 9: Layout of the EMCal.

2.5 Analysis framework

The analysis framework used for simulations and for data analysis makes use of the ROOT framework. This is a C++ based programming environment developed for the NA94 heavy ion experiment that was started in 1994 [9]. The actual framework that is used in ALICE is called AliRoot, which is an ALICE specific extension of ROOT. It is designed to reconstruct and analyse data from real collisions as well as from simulations.

AliRoot has the capability to generate simulations, performing the necessary calculations to simulate the particle interaction at the interaction point, the interaction of particles with the detector hardware and the generated signal in a detector's active surface or volume. The software is designed in layers, where each layer corresponds with a specific phase of data generation, reconstruction and analysis, analogue to the steps of particle collisions, track reconstructing and data analysis in a detector [10].

For producing simulations, the first software layer generates the collision. Libraries such as PYTHIA simulate the production of particles after the collision, along with their momentum and rapidity distribution as they travel from the interaction point.

The second layer makes use of GEANT3. This code simulates the detector response to the generated event. It takes into account the various particle decays, ionizations, multiple scatterings, pair creations, energy depositions and other physical processes that appear when particles traverse the detector. It also stores any new particles that are created in these processes. Each particle (new or already existing) will be kept track of until it either leaves the detector or reaches a momentum threshold.

The third layer takes care of the ALICE specific response to the particle interactions. Here the simulated particle interactions are translated into specific hits in the detectors. Any misalignment in the detector is also taken into account in this step.

From this point the response is formatted in a way that is specific to each detector front-end electronics system and data acquisition system. Hardware noise is also introduced here. The simulated output is very close to the actual output of the operational detector.

The final layer is the analysis reconstruction. Before this point, the data format for real measurements and simulations are different. In the end, both will end up in the same output format. The final layer reconstructs space points, which are used to reconstruct tracks and calculate additional track information such as energy loss, momenta and particle identification. In addition it also stores event specific information such as multiplicity, centrality and the primary vertex.

This information is then stored in a specific format called Event Summary Data (ESD). ESD files from simulated events contain beside the reconstructed information also information about the simulated event, something that is of course not present in the case of real measurements.

At this point user-defined macros can be used to analyse the data in these ESD files and extract the observables that are relevant for the performed analysis. Since the datasets consist of millions of events, the datasets are too large to analyse locally on a single computer. This is why we make use of the GRID, a large distributed computing farm that has datacenters all over the world. Using the GRID greatly reduces the calculation time of the analysis.

3 Heavy flavour electron identification

For this analysis we use a sample of 6.3 million proton-proton collisions. These events were obtained with the ALICE detector in 2011 using an EMCal trigger. This means that the events are recorded when the EMCal detects a photon or electron with sufficiently high enough energy. The trigger level for the EMCal trigger is 4.8 GeV. This trigger allows us to obtain electrons with a higher momentum than if we used a different trigger, but also means that we can not use electrons below that energy.

Since the observables are a function of the transverse momentum p_{T}, the whole analysis is done in 9 p_{T} bins, from 6 GeV/c to 18 GeV/c.

3.1 Event selection

The dataset used for this analysis are EMCal triggered events of period LHC11d. A list of important properties of the dataset can be found below:

- Dataset: LHC11d
- TPC acceptance: $0 < \varphi < 360°$, $|\eta| < 0.9$
- EMCal acceptance: $80 < \varphi < 180°$, $|\eta| < 0.7$
- Run numbers: 156620, 156626, 156629, 156794, 156797, 156829, 156889, 156891, 156896, 157003, 157025, 157203, 157220, 157227, 157257, 157261, 157262, 157275, 157277, 157475, 157476, 157496, 157562, 157564, 157567, 157569, 157734, 157766, 157818, 157819, 157975, 157976, 158086, 158112, 158115, 158118, 158192, 158196, 158200, 158201, 158285, 158287, 158288, 158293, 158301, 158303, 158304, 158526, 158604, 159254, 159258, 159260, 159286, 159318, 159450, 159532, 159535, 159538, 159575, 159577, 159580, 159581, 159582
- Number of events: 6.3 M
- Primary vertex range: $|z| < 10$ cm

3.2 Monte Carlo simulations

For this analysis two different sets of simulations were used. The first sample, LHC11b10b is a π^0 and η enhanced sample at $\sqrt{s} = 2.76$ TeV, anchored to LHC11a. This sample is used for the calculation of the non-HFE reconstruction efficiency. The second sample (LHC12d2) is a 7 TeV pp sample with an enhancement of $c\bar{c}$ and $b\bar{b}$ pairs, used to calculate the azimuthal angular correlation of electrons from charm and beauty mesons as well as the hadron tracking efficiency for comparing the correlation strength with lead-lead measurements.

3.2.1 π^0 and η enhanced sample

The details of this sample are as follows

- Sample: LHC11b10b
- System: proton-proton at $\sqrt{s} = 2.76$ TeV
- Event generator: PYTHIA
- Run numbers: 146686, 146688, 146689, 146746, 146747, 146748, 146801, 146802, 146803, 146804, 146805, 146806, 146807, 146808, 146812, 146813, 146814, 146817, 146824, 146856, 146857, 146858, 146859, 146860
- Number of events: 4.0 M

3.2.2 Heavy flavour enhanced sample

The details of this sample are as follows

- Sample: LHC12d2
- System: proton-proton at $\sqrt{s} = 7$ TeV
- Event generator: PYTHIA
- Run numbers: 156889, 156891, 157275, 157277, 157564, 157734, 158086, 158285, 158287, 158304, 158492, 158516, 158520, 159538, 159580, 159582
- Number of events: 6.3 M

3.3 Track selection

The analysis starts with the identification of electrons. For all the events considered, we only select tracks with a good quality. The cuts on the track quality are specified in table 1.

3.4 Electron identification

The identification of electrons is done with the energy loss measurements of the TPC and the energy measurement of the EMCal.

The TPC gives besides tracking and momentum information of particles also the energy loss while it travels through the TPC. Different species of particles have a different energy loss as function of their momentum. Figure 10 shows

Table 1: Electron candidate track cuts

Track property	**Cut**
Minimum number of ITS clusters	3
Minimum number of TPC clusters	80
Minimum ratio of TPC clusters	0.6
Maximum χ^2 per TPC cluster	4
η range	[-0.9, 0.9]
p_{T} range (GeV/c)	[6, 18]
Reject kink tracks	yes
Require hit in SPD layer	kAny
Require ITS refit	yes
Require TPC refit	yes

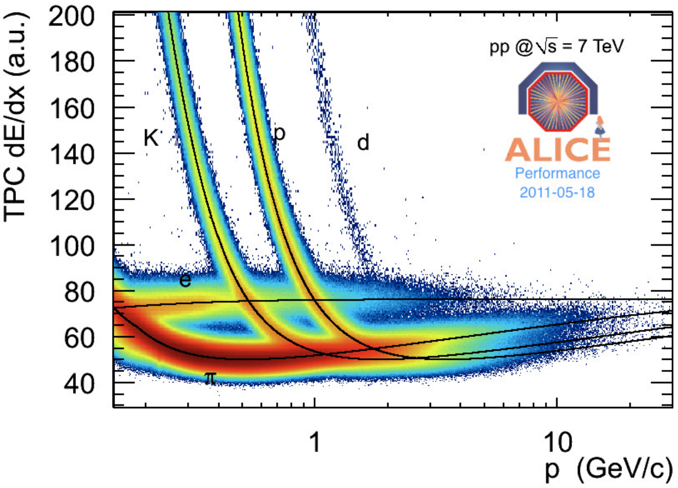

Figure 10: TPC dE/dx distribution as function of momentum for different types of particles. The black lines indicate the Bethe Bloch parametrization.

the energy loss of different types of particles in the TPC. The black lines are the Bethe Bloch parametrization of these distributions [11].

Tracks in the TPC give energy loss and momentum (together with the ITS) information. The closer the measured energy loss lies to the expected value for electrons at that specific momentum, the higher chance that the track is from an electron. For this reason we define the TPC number of sigma's (with respect to electrons), from here on called TPC $N\sigma$:

$$N\sigma = \frac{\text{measured} - \text{expected}}{\text{width}} \quad . \tag{4}$$

Here the width is the width of the energy loss band of electrons. Placing limits on the value of TPC $N\sigma$ each electron candidate can have is the first step of electron identification. In this analysis the tracks with $-1 < N\sigma < 3$ are selected. The TPC $N\sigma$ distribution versus transverse momentum is shown in

Figure 11.

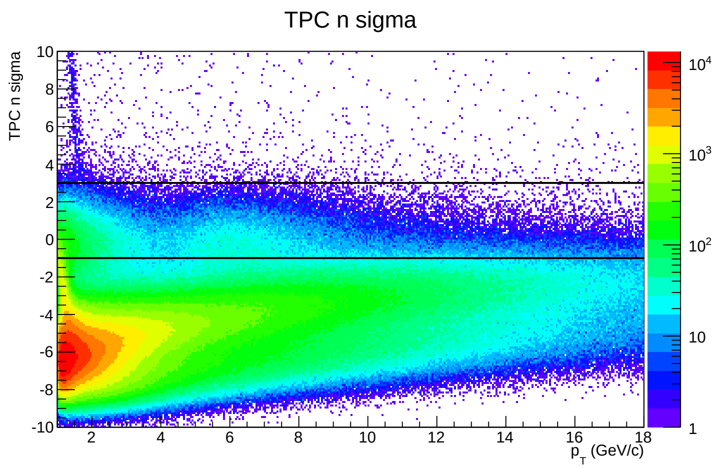

Figure 11: TPC $N\sigma$ distribution of tracks. The black lines represent the cut values.

The next identification step make use of the energy measurement of the EMCal. Since the mass of electrons is low, the energy E and momentum p are nearly equivalent. So cutting on the ratio of these two, E/p removes more hadron tracks from our sample. For this analysis only tracks with $0.8 < E/p < 1.2$ are selected. Figure 12 shows the E/p distribution for tracks with a transverse momentum between 7.5 and 8.5 GeV/c.

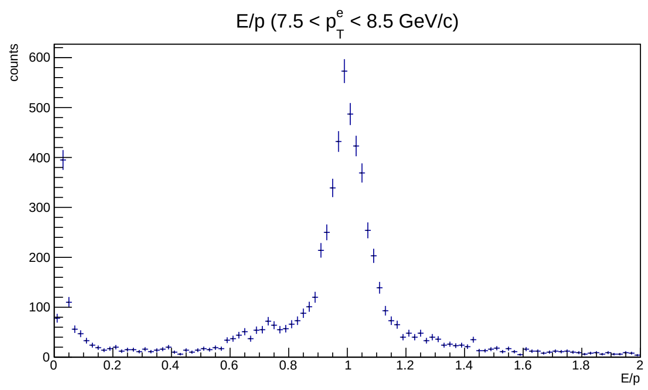

Figure 12: E/p distribution of tracks with $7.5 < p_{\mathrm{T}} < 8.5$ GeV/c after TPC n sigma cut and before the application of shower shape cuts.

The final identification step is a cut on the shape of the electromagnetic shower that the track leaves in the EMCal. Tracks in the ITS and TPC are propagated to the EMCal detector, where they are matched with reconstructed electromagnetic showers in the EMCal. If the distance between the track projection on the surface of the EMCal and the reconstructed shower has $\Delta\eta < 0.025$ and $\Delta\varphi < 0.05$ the track is accepted. The shape of the shower is different for electrons than for hadrons, so cutting on this shape further improves our electron sample. The cut values are placed on the short axis (M20) and long axis (M02) of the shower shape. The limits are M20 < 0.2 and M02 < 0.5. Figure 13 shows the effect of the application of these cuts, by comparing the E/p distribution before and after.

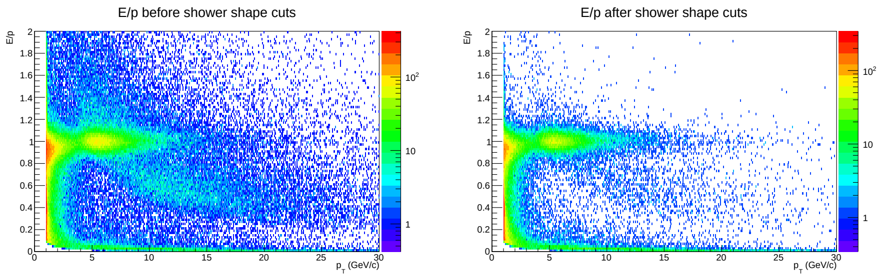

Figure 13: E/p distribution after applying a TPC $N\sigma$ cut, before (left panel) and after (right panel) applying shower shape cuts.

After all these cuts we have an electron sample with high purity (see Section 3.5). These electrons are called the inclusive electrons.

3.4.1 Cut optimization

In order to determine the most optimal cuts values for TPC $N\sigma$ and shower shape, 4 sets were defined. They are summarized in Table 2. The E/p distributions after applying these cuts were compared to see the most optimal set. These distributions are shown in Figure 14 for the different p_{T} bins. It was decided to use set 3, since set 1 leaves a lot of hadron contamination in the sample, set 4 removes too much signal and set 2 has nearly the same effect on the distribution as set 3.

Table 2: The values of the different cut sets.

Cut set	**TPC $N\sigma$**	**M20**	**M02**
1	[-1,3]	< 0.3	< 0.7
2	[-0.5,3]	< 0.3	< 0.7
3	[-1,3]	< 0.2	< 0.5
4	[-0.5,3]	< 0.2	< 0.5

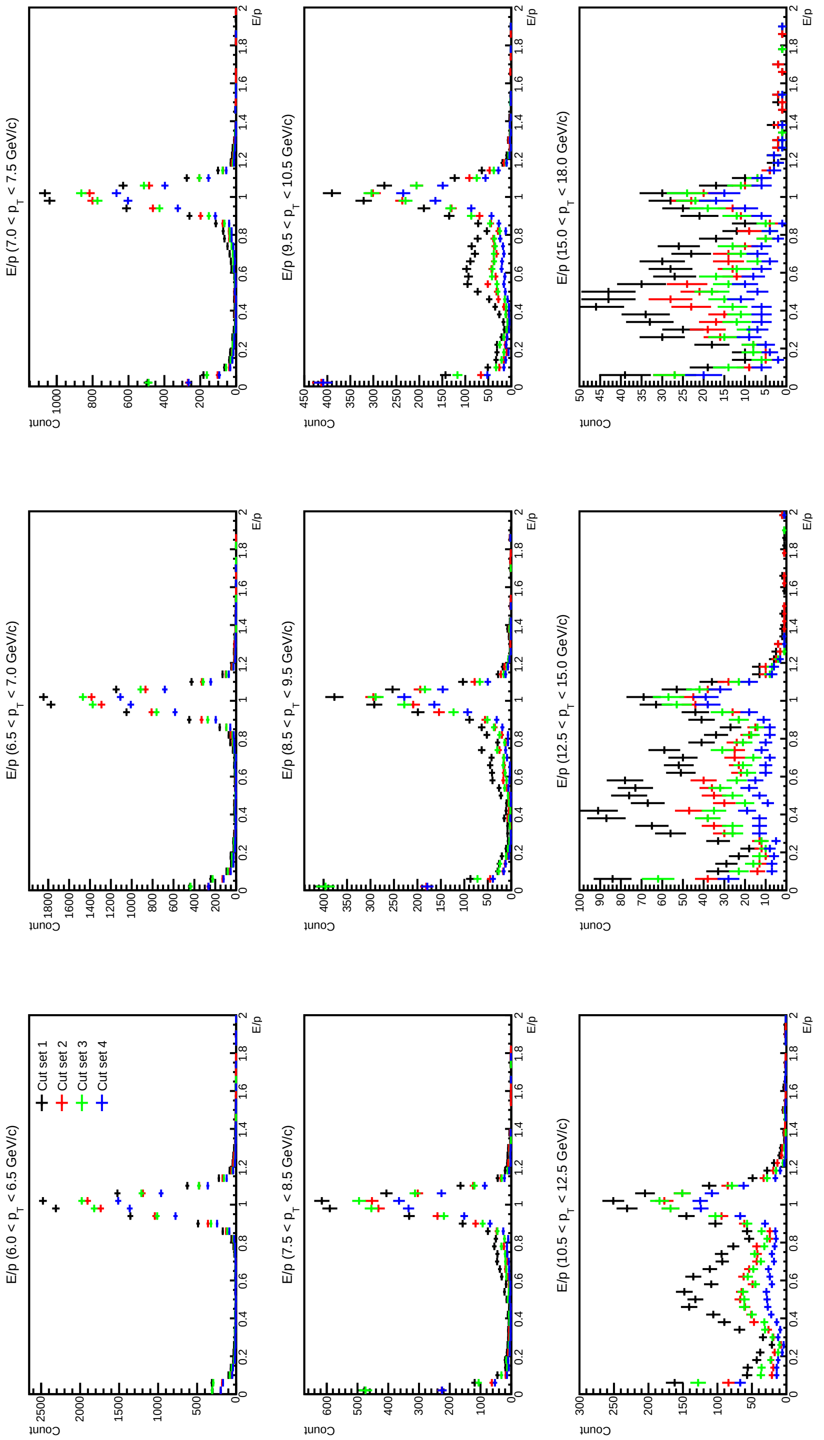

Figure 14: E/p distribution for the different cut sets (see Table 2) and different $p_{\rm T}$ bins.

3.5 Hadron contamination

The inclusive electron sample does not contain purely electrons, it is contaminated by some hadrons that remain after applying electron identification cuts. This contamination is determined by looking at the E/p distribution for tracks with a TPC $N\sigma$ range outside of the range for electrons (after applying the same shower shape cuts): by taking tracks with $-8 <$ TPC $N\sigma < -4$ and scaling it to the E/p for $-1 <$ TPC $N\sigma < 3$ between 0 and 0.8. As an example Figure 15 shows both distributions for the p_{T} bin of 10.5-12.5 GeV/c. From this plot the contamination is determined by integrating both distributions between the E/p cut range [0.8,1.2] and dividing the hadron integral over the electron integral. The purity is defined as 1-contamination and is shown in Figure 16. It decreases from 96% in the first p_T bin to 74% in the last bin. This hadron contamination is removed from the inclusive electron sample.

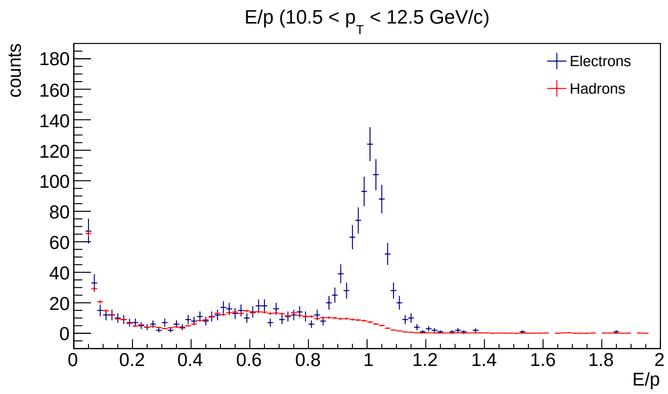

Figure 15: E/p distribution for hadrons ($-8 <$ TPC $N\sigma < -4$, red points) and electrons ($-1 <$ TPC $N\sigma < 3$, blue points) after applying shower shape cuts for momentum between 10.5 and 12.5 GeV/c. The hadron distribution is scaled to match the electron distribution between 0 and 0.8.

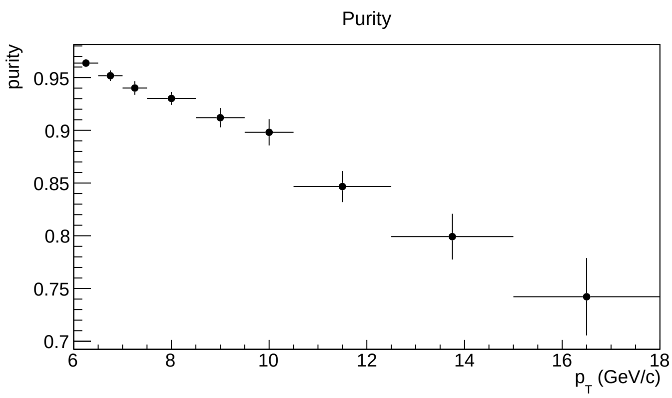

Figure 16: Electron purity as a function of transverse momentum.

To ensure that only the electrons that triggered the events are selected, we select only those that have EMCal clusters matching the EMCal trigger cluster.

3.6 Non-heavy flavour electron reconstruction

The inclusive electron sample contains electrons from different sources. The electrons of interest are the heavy flavour decay electrons (HFE), coming from the semi-leptonic decay of D and B mesons. Other sources of electrons are Dalitz decay and conversion of photons. We call these electrons non-heavy flavour electrons (non-HFE or NHFE). We can use the fact that non-heavy flavour electrons always come in pairs of electron-positron to separate the HFE from the non-HFE. The opening angle and invariant mass of e^+ and e^- pairs from non-HFE decays is very small while no such correlation exists for heavy flavour electrons. Thus the non-HFE background can be reconstructed by pairing the $e^\pm$ and their opposite-charge-sign partners and calculating their opening angle and invariant mass and placing cuts on them.

However, some electrons might be HFE but be accidentally marked as non-HFE by this method. This happens if an electron and positron with opposite sign form a pair that is below the opening angle and invariant mass cut by coincidence. This contribution is the called the combinatorial background and can be estimated by looking at the opening angle and invariant mass distribution of tracks with the same charge sign, because for these like sign pairs the only contribution is this combinatorial background.

After finding the electrons in an event, we loop again over all other tracks in the same event to find the partner $e^\pm$. In order to find the partner electrons with a high efficiency, we apply a loose TPC $N\sigma$ cut on them. The cuts that are applied to these associated tracks are summarized in Table 3. Before applying a cut on the invariant mass, first a cut on the opening angle is placed.

The opening angle distribution of like sign (LS) and unlike sign (ULS) pairs is shown in Figure 17. As indicated by the black line, pairs with an opening angle above 0.2 rad are rejected.

The invariant mass distribution for ULS and LS pairs that pass the opening angle cut is shown in Figure 18. The cut placed on the invariant mass is $m < 0.1$ GeV/c^2.

Table 3: Associated electron candidate track cuts

Track property	**Cut**
Minimum number of TPC clusters	80
Maximum χ^2 per TPC cluster	3.5
η range	[-0.9, 0.9]
Minimum p_T	0.3 GeV/c
Reject kink tracks	yes
Require TPC refit	yes
TPC $N\sigma$ (w.r.t. electron dE/dx)	[-3, 3]

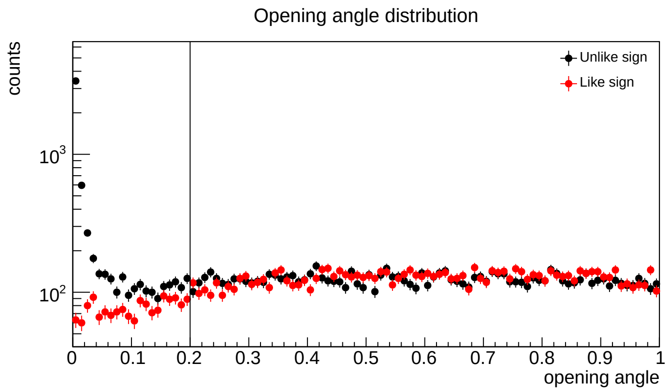

Figure 17: Opening angle of LS and ULS electron pairs. The black line indicates the cut value.

3.7 Non-heavy flavour electron reconstruction efficiency

Since we do not reconstruct every electron in an event, if one of the two $e^{\pm}$ of a non-HFE pair is not reconstructed, it will be wrongly marked as being HFE. We can correct for this fact, but need the non-HFE reconstruction efficiency for this. This efficiency is calculated using a Monte Carlo sample. A Monte Carlo sample does not contain real measurements, but is simulated. This is done by first generating the event with an event generator (PYTHIA in this case), and next is propagated through the detector, using GEANT which simulates the detector response. The sample that is used in this case is a π^0 and η enhanced sample, which means that on top of the normal generation, there are extra π^0 and η mesons added, which eventually decay to electron-positron pairs. Without this enhancement there are far more simulations required to have an accepted level of statistic.

The enhancement introduces a bias on the p_{T} distribution of electrons. This bias is removed by calculating the enhancement factor of π^0 and η and applying it as a weight to the p_{T} distribution of electrons. Figure 19 shows the non-HFE reconstruction efficiency before and after applying the weight. In the momentum region of our analysis the reconstruction efficiency is roughly 70%.

The Monte Carlo sample that was used for this analysis was generated with a center-of-mass energy of $\sqrt{s}$ = 2.76 TeV. The production of a $\sqrt{s}$ = 7 TeV sample was requested, but has been suffering from technical issues. However, a first working test production of the simulations at 7 TeV show that both efficiencies agree with each other within the statistical error, which can be seen in Figure 20. Since this was a test production with a small number of events and thus a large statistical error, the 2.76 TeV sample was used instead.

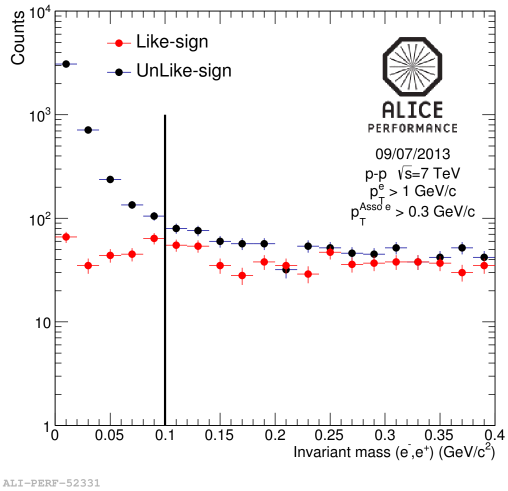

Figure 18: Invariant mass distribution of LS and ULS electron pairs after applying an opening angle cut of 0.2 rad. The black line indicates the cut value.

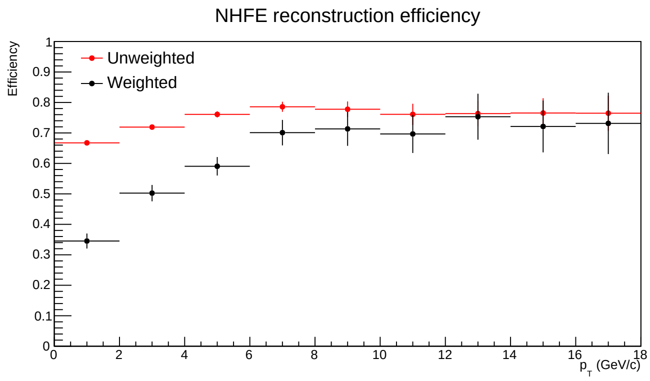

Figure 19: The non-heavy flavour electron reconstruction efficiency before (red points) and after (black points) applying the weight.

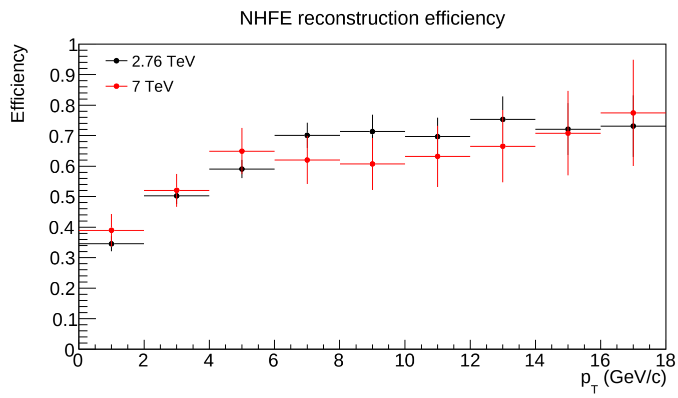

Figure 20: The non-heavy flavour electron reconstruction efficiency for $\sqrt{s}$ = 2.76 and 7 TeV. Both efficiencies agree with each other within statistical errors.

4 Azimuthal angular correlations of heavy flavour electrons and charged hadrons

We start with the number of inclusive electrons, $N_{\mathrm{e}}^{\mathrm{incl}}$, using the electron identification and track cuts explained in the previous section. The hadron contamination is estimated using the scaled E/p distributions for hadrons and removed from the sample. If we define the purity as p, the number of hadrons is given by:

$$N_{\mathrm{h}} = (1-p)N_{\mathrm{e}}^{\mathrm{incl}} \quad . \tag{5}$$

The non-heavy flavour electron contribution is estimated by the number of unlike sign pairs, $N_{\mathrm{e}}^{\mathrm{ULS}}$. Some of the true heavy flavour electrons are reconstructed by accident as non-heavy flavour electrons by the invariant mass method. We can estimate this number from the invariant mass of like sign pairs, $N_{\mathrm{e}}^{\mathrm{LS}}$. The number of reconstructed non-heavy flavour electrons is then given by

$$N_{\mathrm{e}}^{\mathrm{NHF,\,reco}} = N_{\mathrm{e}}^{\mathrm{ULS}} - N_{\mathrm{e}}^{\mathrm{LS}} \quad . \tag{6}$$

The sample also contains non-heavy flavour electrons that are not reconstructed as such. This can be estimated by using the non-heavy flavour reconstruction efficiency ϵ^{NHFE}:

$$N_{\mathrm{e}}^{\mathrm{NHF,\,not\ reco}} = \left(\frac{1}{\epsilon^{\mathrm{NHFE}}} - 1\right) N_{\mathrm{e}}^{\mathrm{NHF,\,reco}} \quad . \tag{7}$$

Thus the heavy flavour electron yield can be expressed as

$$N_{\mathrm{e}}^{\mathrm{HF}} = p\, N_{\mathrm{e}}^{\mathrm{incl}} - N_{\mathrm{e}}^{\mathrm{NHF,\,reco}} - N_{\mathrm{e}}^{\mathrm{NHF,\,not\ reco}} \quad . \tag{8}$$

The azimuthal angular correlations between heavy flavour electrons and hadrons are then calculated by

$$\begin{aligned}\frac{\mathrm{d}N^{\mathrm{HF}}}{\mathrm{d}\Delta\varphi_{\mathrm{e-h}}} =& \frac{\mathrm{d}N^{\mathrm{incl}}}{\mathrm{d}\Delta\varphi_{\mathrm{e-h}}} - \frac{\mathrm{d}N^{\mathrm{ULS}}}{\mathrm{d}\Delta\varphi_{\mathrm{e-h}}} + \frac{\mathrm{d}N^{\mathrm{LS}}}{\mathrm{d}\Delta\varphi_{\mathrm{e-h}}} \\ & - \left(\frac{1}{\epsilon^{\mathrm{NHFE}}} - 1\right)\left(\frac{\mathrm{d}N^{\mathrm{ULS,\,no\ partner}}}{\mathrm{d}\Delta\varphi_{\mathrm{e-h}}} - \frac{\mathrm{d}N^{\mathrm{LS,\,no\ partner}}}{\mathrm{d}\Delta\varphi_{\mathrm{e-h}}}\right) \quad ,\end{aligned} \tag{9}$$

where each of the $\Delta\varphi$ distributions on the right hand side of the equation are determined experimentally. The $\mathrm{d}N^{\mathrm{incl}}/\mathrm{d}\Delta\varphi_{\mathrm{e-h}}$ is the correlation of every electron in the sample, and is corrected for the hadron contamination by subtracting the hadron-hadron correlation per trigger multiplied by the number of hadrons N_{h}, as shown in Figure 21. Electrons that form a unlike sign or like sign pair are correlated with hadrons to form $\mathrm{d}N^{\mathrm{ULS}}/\mathrm{d}\Delta\varphi_{\mathrm{e-h}}$ and $\mathrm{d}N^{\mathrm{LS}}/\mathrm{d}\Delta\varphi_{\mathrm{e-h}}$, respectively. Figure 22 shows these distributions. The final two terms of Equation 9 represent the not reconstructed non-HFE, so these are the unlike sign and like sign correlation distributions where we remove the partner electron. These distributions are shown in Figure 23.

The hadron track selection cuts that are used for these correlation distributions are summarized in Table 4.

Table 4: Hadron track cuts

Track property	**Cut**
Minimum number of TPC clusters	80
Maximum χ^2 per TPC cluster	3.5
η range	[-0.9, 0.9]
Minimum p_{T}	0.3 GeV/c
Reject kink tracks	yes
Require ITS refit	yes
Require TPC refit	yes

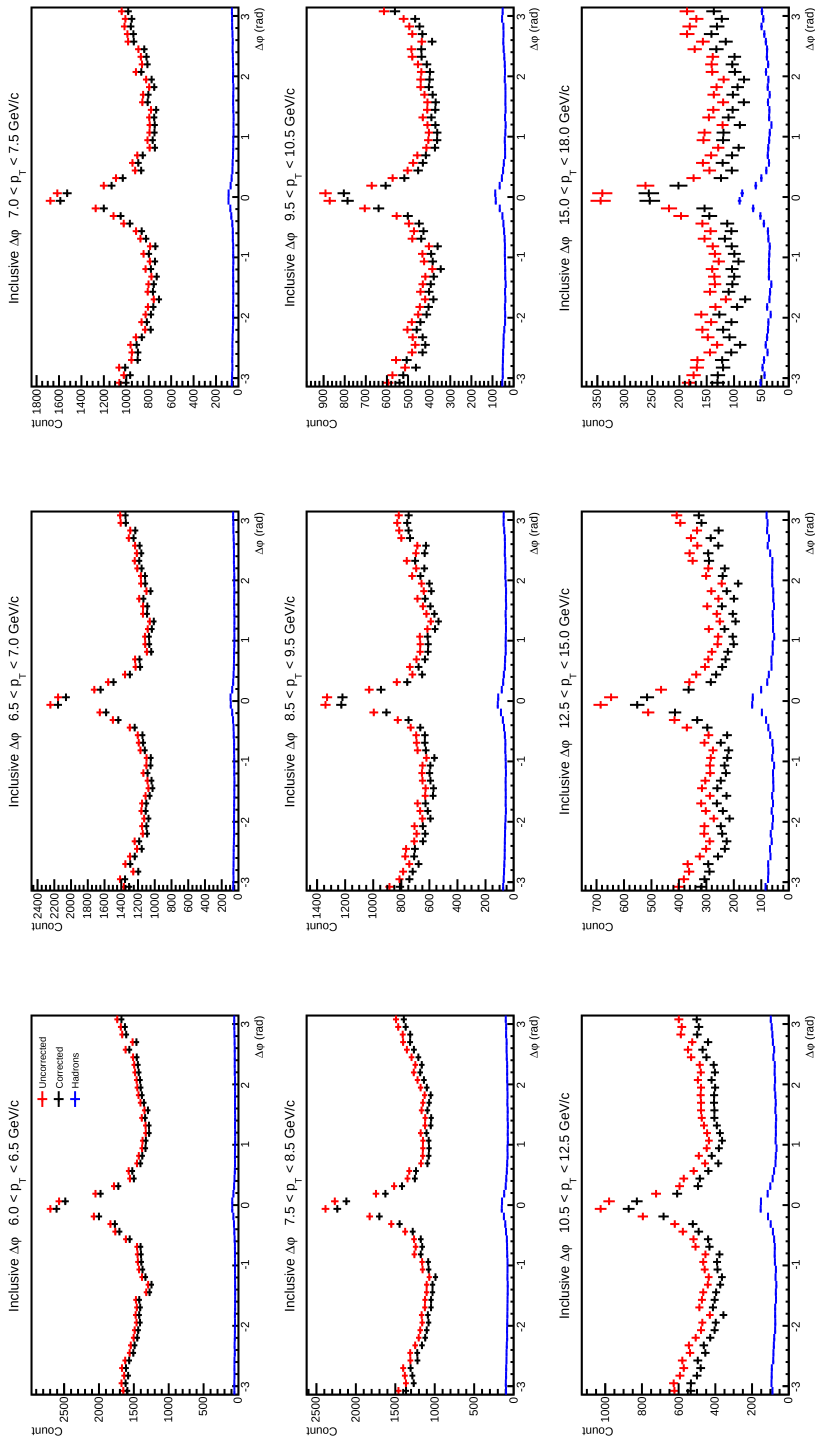

Figure 21: Azimuthal angular correlations for inclusive electrons (red), which is then corrected by the scaled hadron-hadron angular correlation (blue) to get the corrected distribution (black).

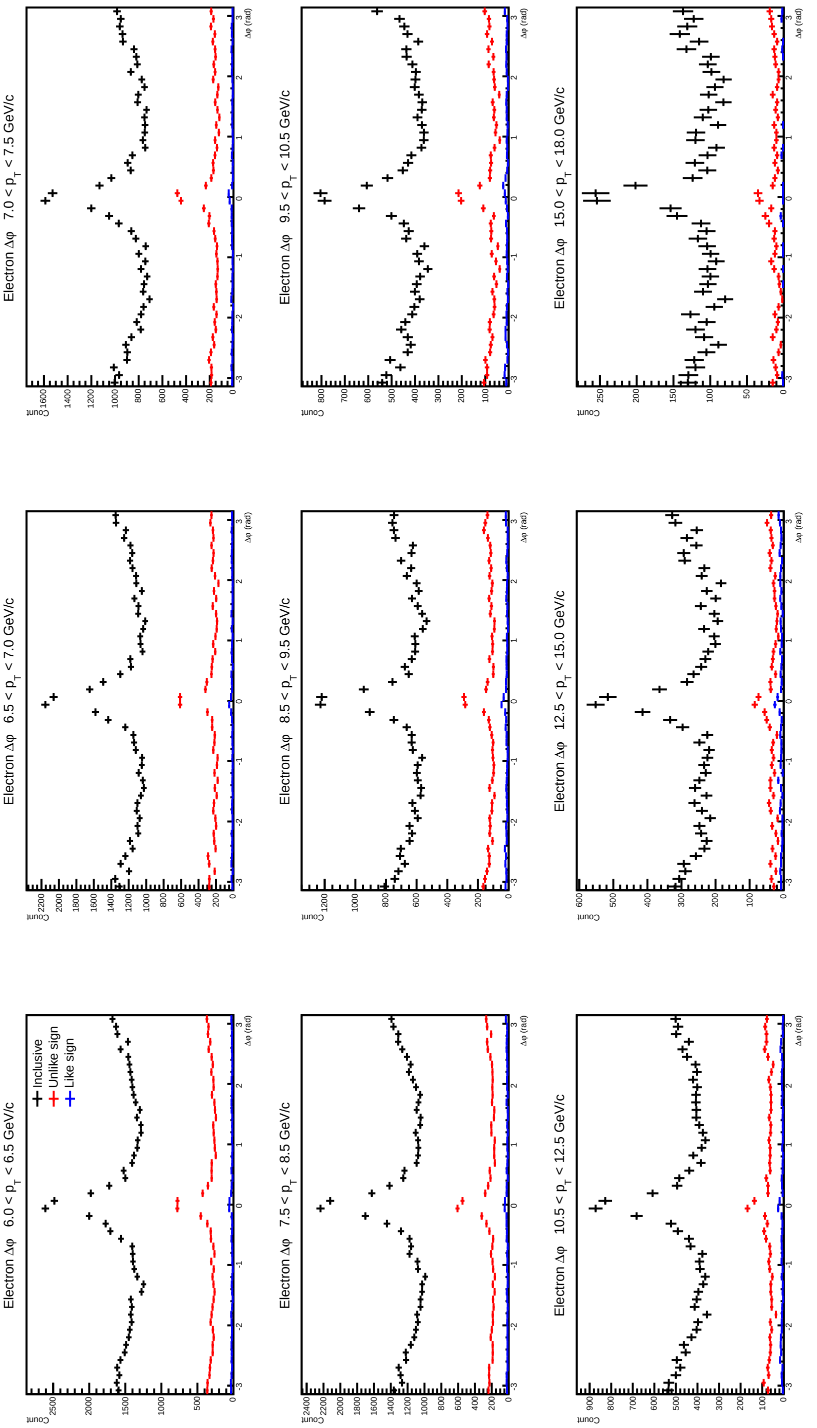

Figure 22: Azimuthal angular correlations for inclusive electrons (black), electrons that form an ULS pair (red) and electrons that form a LS pair (blue).

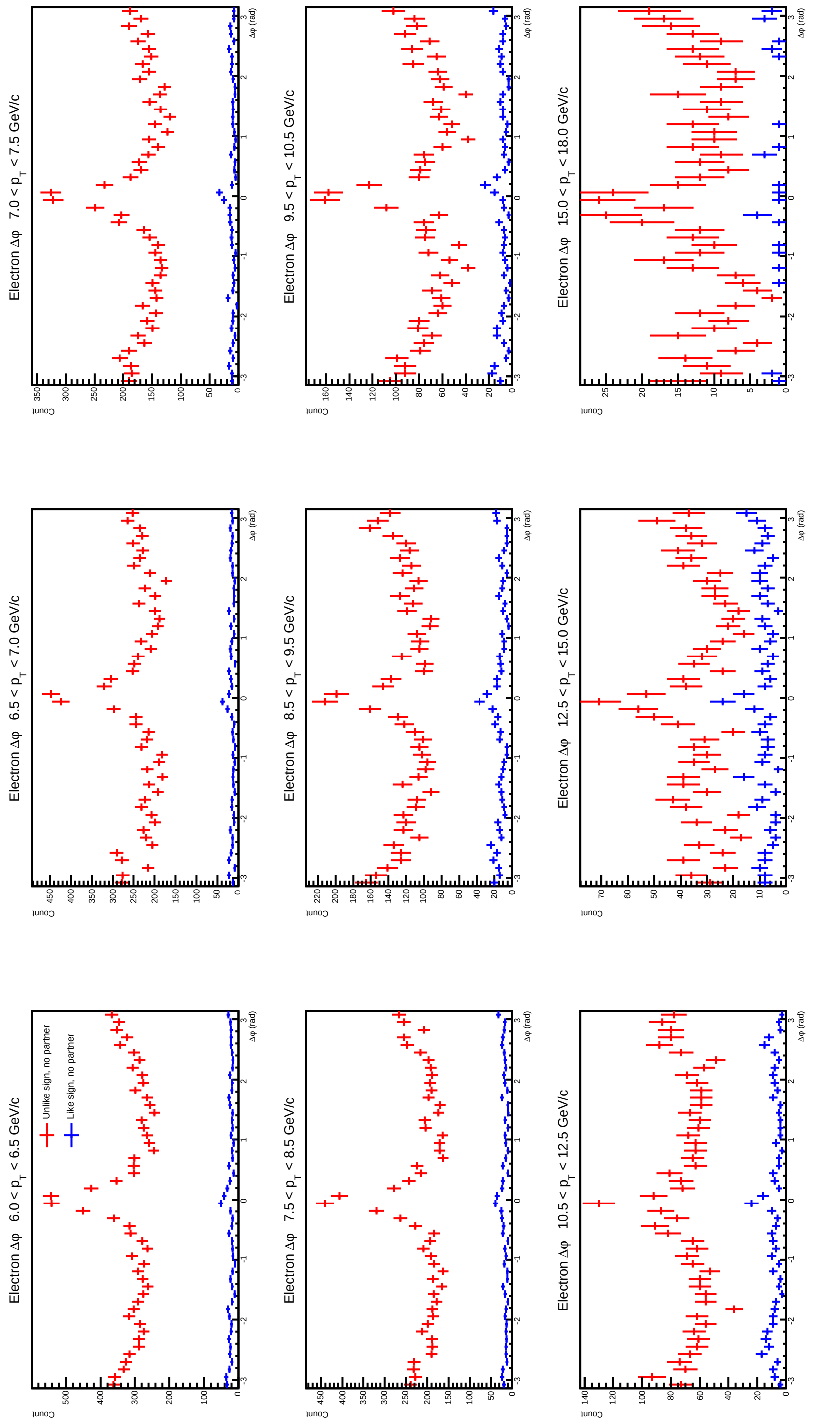

Figure 23: Azimuthal angular correlations for electrons that form an ULS pair (red) and electrons that form a LS pair (blue). Here the partner electrons are removed from the ULS and LS distributions.

5 Relative beauty contribution to heavy flavour electron spectra

The sample of heavy flavour electrons we have contains both electrons from semi-leptonic decay of B and D mesons. The fraction of electrons that come from B is defined as r_{B}, thus we have the expression

$$N_{\mathrm{e}}^{\mathrm{HF}} = r_{\mathrm{B}} N_{\mathrm{e}}^{\mathrm{B}} + (1 - r_{\mathrm{B}}) N_{\mathrm{e}}^{\mathrm{D}} \ . \tag{10}$$

Here $N_{\mathrm{e}}^{\mathrm{B}}$ and $N_{\mathrm{e}}^{\mathrm{D}}$ are the number of electrons that come from B and D decay, respectively. But this equation does not allow us to calculate the beauty fraction, since we do not know any term on the right hand side.

However, since the mass of the beauty quark is about 3 times higher than the mass of the charm quark, the shower that contains an electron from B (which contains a b quark) is wider than when it contains an electron from D (which contains a c quark). Monte Carlo simulations allow us to calculate the shape of these two distributions. To calculate the ratio of electrons from beauty decays, the heavy flavour electron azimuthal angular correlation distribution is fitted with

$$\frac{\mathrm{d}N^{\mathrm{HF}}}{\mathrm{d}\Delta\varphi_{\mathrm{e-h}}} = c + r_{\mathrm{B}} \frac{\mathrm{d}N^{\mathrm{B}}}{\mathrm{d}\Delta\varphi_{\mathrm{e-h}}} + (1 - r_{\mathrm{B}}) \frac{\mathrm{d}N^{\mathrm{D}}}{\mathrm{d}\Delta\varphi_{\mathrm{e-h}}} \ . \tag{11}$$

The two fit parameters are the beauty fraction r_{B} and a constant c which is the uncorrelated background, which is expected to be flat in pp collisions. $\mathrm{d}N^{\mathrm{D}}/\mathrm{d}\Delta\varphi_{\mathrm{e-h}}$ and $\mathrm{d}N^{\mathrm{B}}/\mathrm{d}\Delta\varphi_{\mathrm{e-h}}$ are azimuthal angular correlation between electrons from D and B meson decay respectively and charged hadrons from Monte Carlo simulations with full detector simulations. These two distributions are called the fitting templates. The simulations used to obtain these correlation distributions is a heavy flavour electron enhanced sample generated with PYTHIA. Heavy flavour electron enhanced means every event contains at least one $c\bar{c}$ or $b\bar{b}$ pair, which is then forced to a semi-leptonic decay after hadronization.

The fitting range is $-1.5 < \Delta\varphi < 1.5$ rad. We only fit on the near side of the peak since on the away-side is not simulated correctly by PYTHIA.

All distributions are normalized by the number of electrons that are used to calculate the distribution. We call this the number of triggers. For the measured distribution the number of triggers is calculated with Equation 8.

Figure 24 shows the correlation distributions normalized per trigger for the different p_{T} bins together with the distributions from D and B meson decay and the fit of (11).

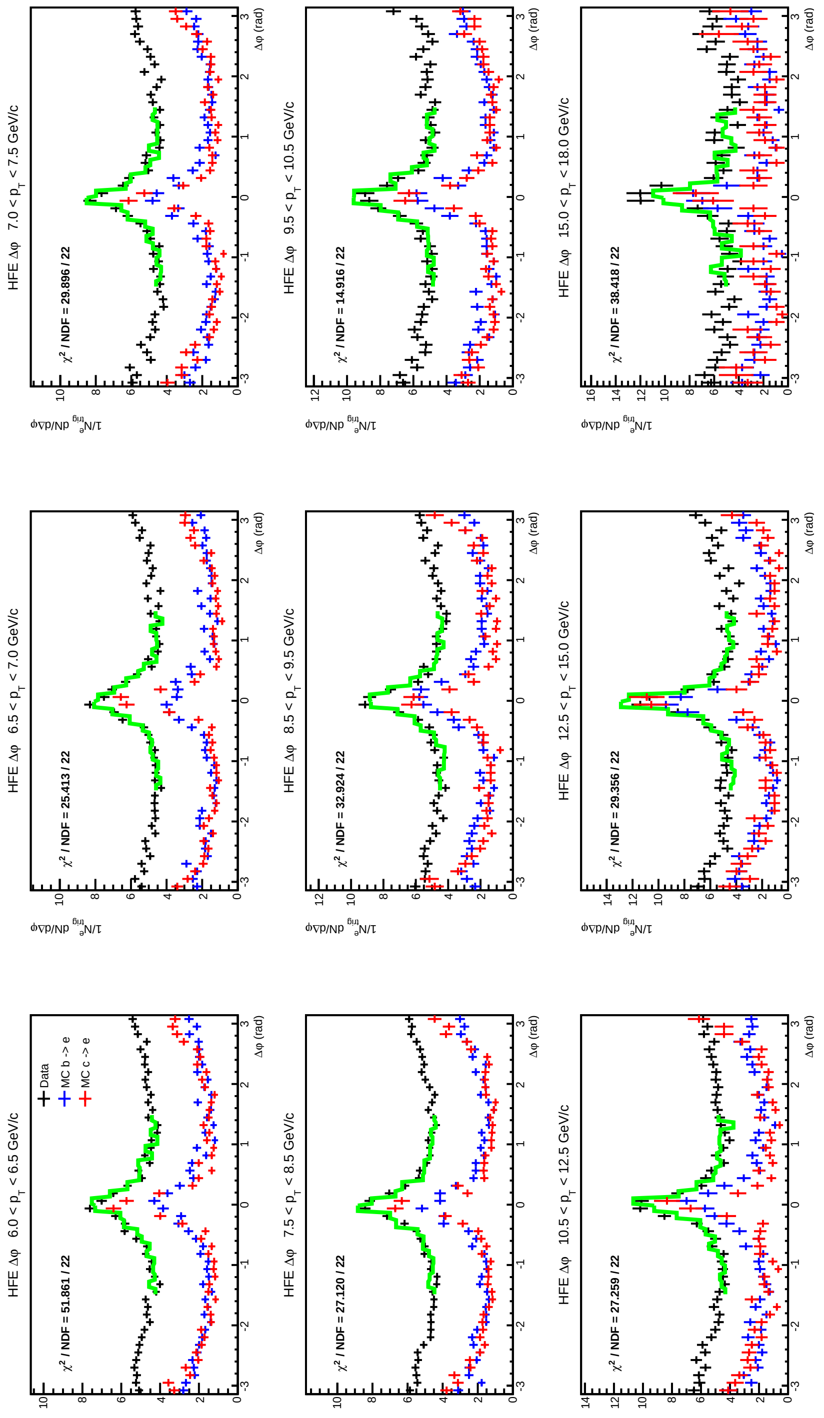

Figure 24: Azimuthal angular correlations between heavy flavour decay electrons and charged hadrons (black points) for the different p_T bins. The red and blue points are the correlation distributions obtained from Monte Carlo simulations for electrons from D and B meson decays. The green line is the fit to the data.

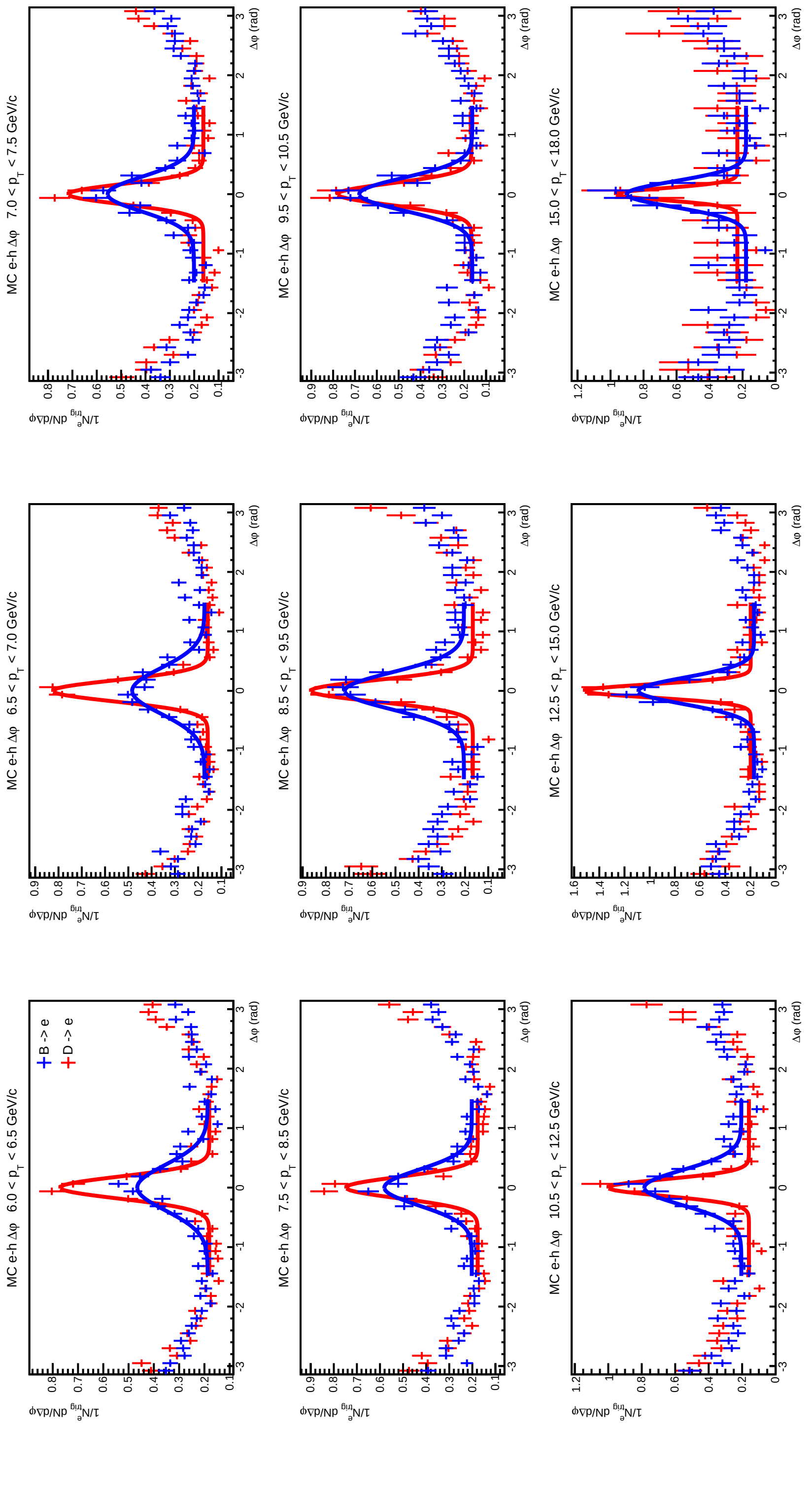

Figure 25: Azimuthal angular correlations for electrons from D (red) and B (blue) meson decays. The solid lines are the a Gaussian fit to the distributions.

5.1 Template momentum range

At high p_{T} ($\gtrsim$ 10 GeV/c), the width of the correlation distributions for electrons from D and B meson decay become similar. At this point our method of measuring r_{B} breaks down. To check if this method is still usable at our highest momentum bins, both Monte Carlo correlation distributions are fitted with a Gaussian on the near side and their widths are compared. The templates and their fits are shown in Figure 25. The widths of these distributions and their difference is shown in Figure 26. These figures show a clear difference in width of the two templates, which allows to use this method to extract r_{B} up to 18 GeV/c.

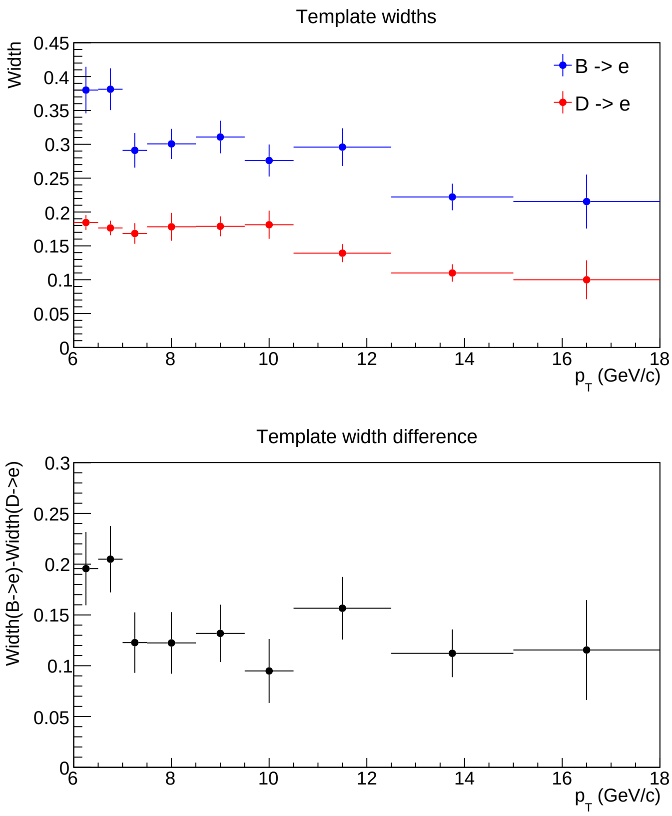

Figure 26: The width (upper panel) and width difference (lower panel) of the near-side correlation between electrons from B and D meson decay and hadrons.

6 Baseline measurement for comparison with lead-lead data

The correlation distribution from pp collisions at 7 TeV is used as a baseline measurement for Pb-Pb collisions. To offer a fair comparison, the analysis for pp and Pb-Pb collision have to be in the same kinematic range, i.e. they have to have the same momentum cuts. In the Pb-Pb analysis the bins are split up in 3 electron p_{T} ranges, each with 2 hadron p_{T} ranges. So for the comparison this is also done in our analysis.

The extracted yields have to be corrected for the fact that not all hadrons are reconstructed. The fraction of hadron tracks that are reconstructed is known as the tracking efficiency. The tracking efficiency is calculated using the heavy flavour electron enhanced Monte Carlo sample and is defined as

$$\epsilon_{\mathrm{tracking}} = \frac{\text{All reconstructed hadron tracks}}{\text{All physical primary hadron tracks}} \quad . \tag{12}$$

The same hadron track cuts as in the measurements are applied. Figure 27 shows the tracking efficiency as function of hadron transverse momentum. The two vertical red lines indicate the ranges of hadron p_{T} we are using.

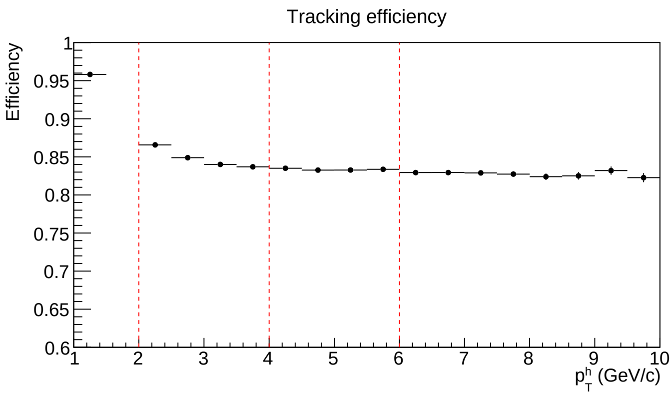

Figure 27: Tracking efficiency of hadrons as function of hadron p_{T}. The red lines indicate the two hadron p_{T} bins that are used.

After correcting for the tracking efficiency, the HFE correlation distribution is fitted with a Gaussian distribution on the near-side with the mean fixed at zero and a constant pedestal. The analysis is done in two separate hadron p_{T} bins. Figure 28 shows the correlation distribution for $2 < p_{\mathrm{T}}^{\mathrm{h}} < 4$ GeV/c together with the fit and Figure 29 shows the same for $4 < p_{\mathrm{T}}^{\mathrm{h}} < 6$ GeV/c. From the Gaussian fit the yield and width of the correlation function are extracted. The extracted yield and width are shown in Figure 30 for $2 < p_{\mathrm{T}}^{\mathrm{h}} < 4$ GeV/c and Figure 31 shows $4 < p_{\mathrm{T}}^{\mathrm{h}} < 6$ GeV/c.

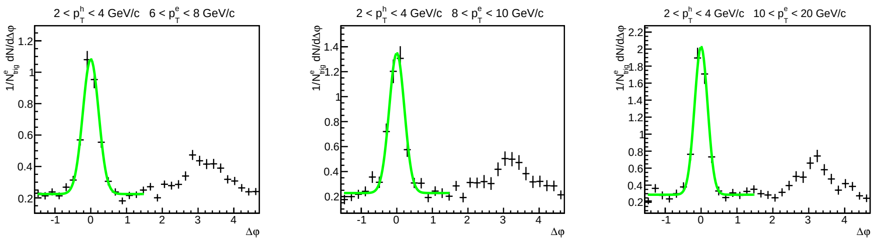

Figure 28: Azimuthal angular correlation between heavy flavour decay electrons and hadrons, with hadron p_{T} between 2 and 4 GeV/c. The green line is a Gaussian fit to the near-side peak.

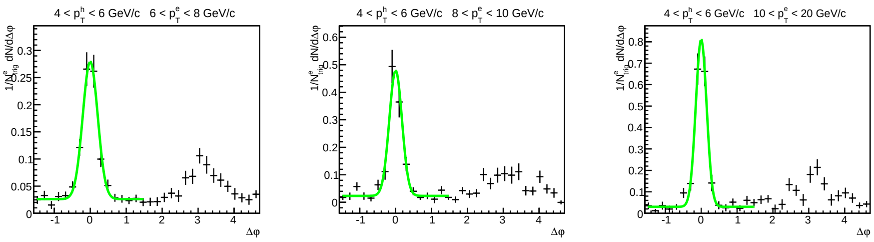

Figure 29: Azimuthal angular correlation between heavy flavour decay electrons and hadrons, with hadron p_{T} between 4 and 6 GeV/c. The green line is a Gaussian fit to the near-side peak.

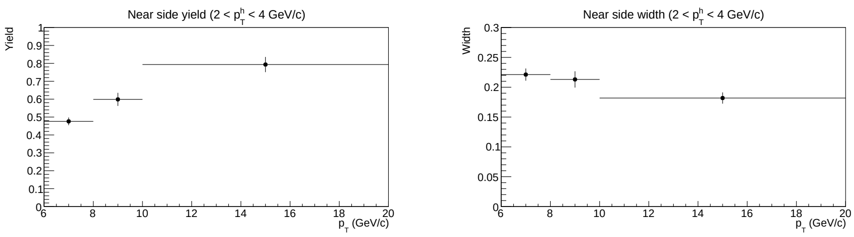

Figure 30: The near-side yield (left panel) and width (right panel) from the heavy flavour electron correlation distribution with hadron p_{T} between 2 and 4 GeV/c.

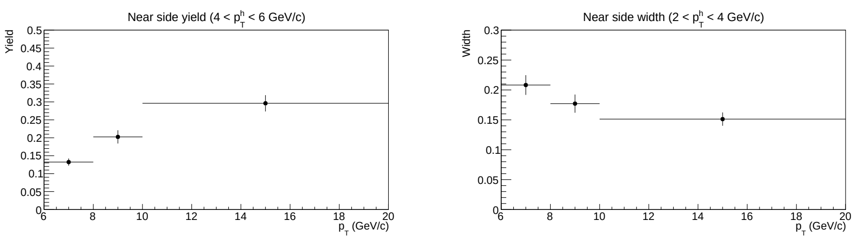

Figure 31: The near-side yield (left panel) and width (right panel) from the heavy flavour electron correlation distribution with hadron p_{T} between 4 and 6 GeV/c.

7 Systematic uncertainties

The measured values might slightly depend on the way the analysis was done. For example if one of the cuts was slightly different, the results might vary as well. This uncertainty is called the systematic uncertainty and can be accounted for by varying different cut parameters of the analysis and looking at their effect on the relative beauty fraction r_{B} and the yield separately. The analyzed systematics are:

- Electron identification (Figure 32 and 37)
  - TPC $N\sigma$ cut
  - E/p cut
  - Shower shape cuts
  - Minimum number of TPC clusters
- Non-heavy flavour electron estimation (Figure 33 and 38)
  - Opening angle cut
  - Invariant mass cut
  - Reconstruction efficiency
  - Minimum number of TPC clusters on the associated electron
- Hadron cuts (Figure 34 and 39)
  - Hadron minimum p_{T} (only for r_{B})
  - Minimum number of TPC clusters on the hadrons
  - Using 2.76 TeV MB tracking efficiency (only for baseline)
- Fitting procedure (Figure 35 and 40)
  - Fitting range (only for r_{B})
  - Not fixing mean (only for baseline)
  - Bin counting (only for baseline)
  - Fixing pedestal from fitting it first (only for baseline)
- Gluon splitting rate (only for r_{B}) (Figure 36)
- Momentum resolution (only for baseline) (Figure 41)

The last two systematic sources are more than simply changing some parameters in the analysis, which is why they are explained in more details in the next subsections.

The total systematic is calculated by adding the separate sources in quadratic:

$$(sys_{\mathrm{total}})^2 = \sum_i (sys_i)^2 \quad . \tag{13}$$

Table 5 and 6 contain the result of the study of sources of systematic uncertainty.

7.1 Figures for systematic error evaluation for relative beauty fraction

In this section the figures from which the systematic errors on r_{B} are determined are shown. The black lines represent the assigned systematic for each of the sources.

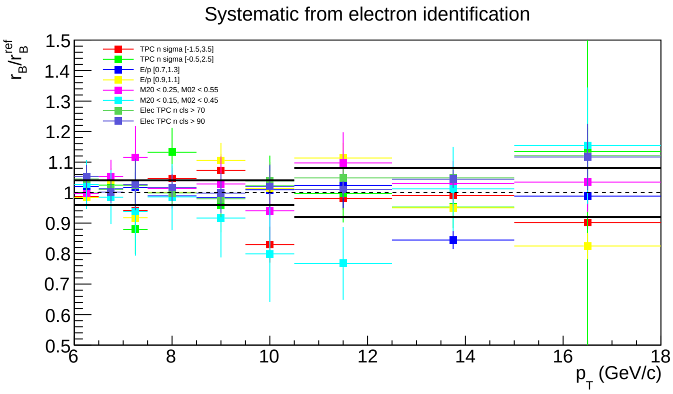

Figure 32: Systematics on the electron identification for r_{B}. The solid horizontal lines represent the assigned systematic.

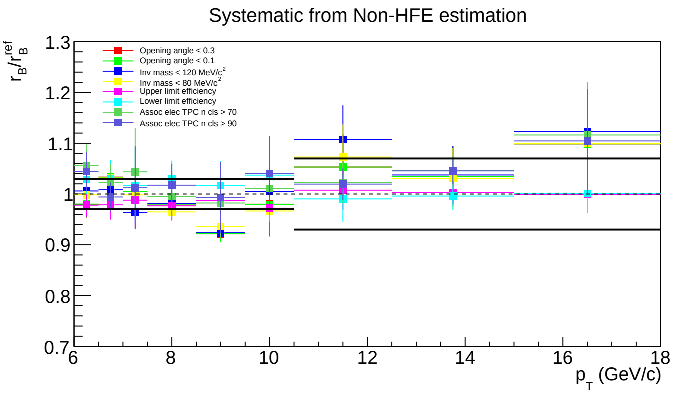

Figure 33: Systematics on the non-heavy flavour electron estimation for r_{B}. The solid horizontal lines represent the assigned systematic.

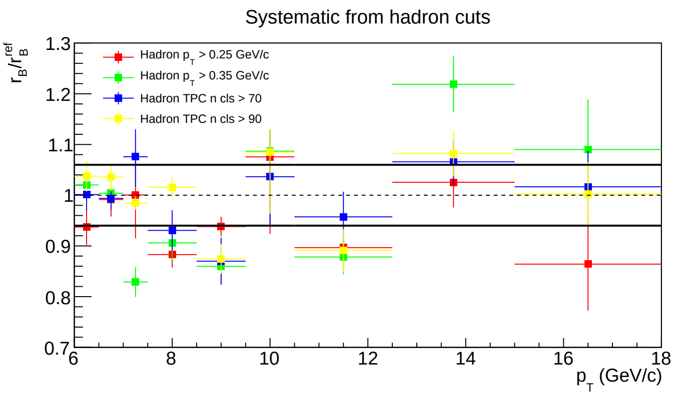

Figure 34: Systematics on the hadrons for r_{B}. The solid horizontal lines represent the assigned systematic.

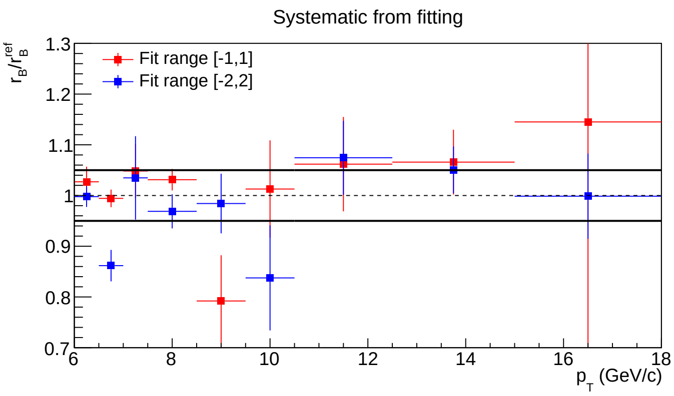

Figure 35: Systematics on the fitting procedure for r_{B}. The solid horizontal lines represent the assigned systematic.

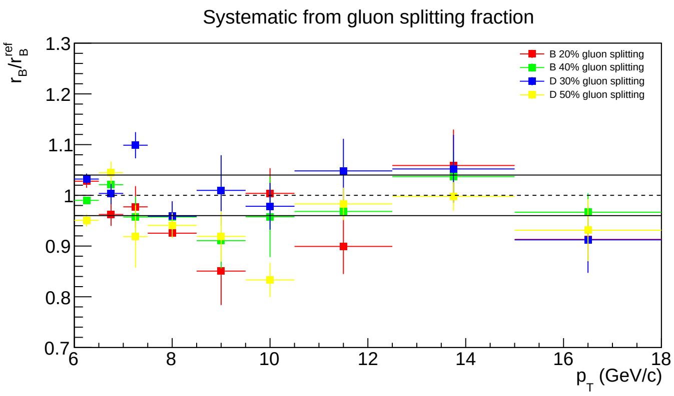

Figure 36: Systematics on the gluon splitting fraction of the template. The solid horizontal lines represent the assigned systematic.

7.2 Figures for systematic error evaluation for baseline measurement

In this section the figures from which the systematic errors on the yield are determined are shown. The black lines represent the assigned systematic for each of the sources.

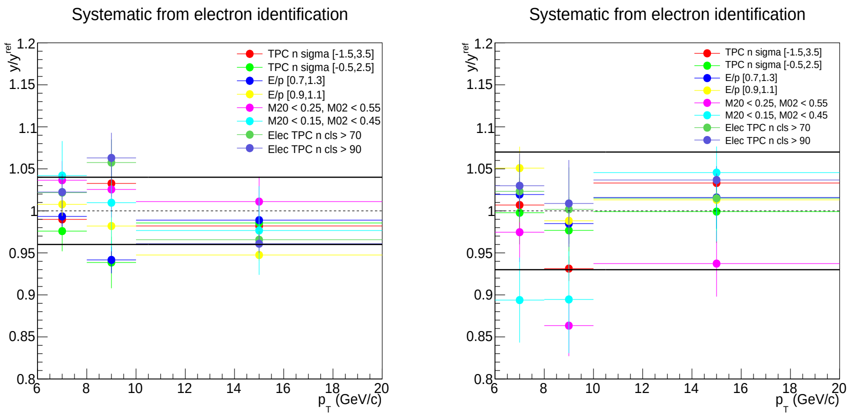

Figure 37: Systematics on the electron identification for $2 < p_{\mathrm{T}}^{\mathrm{h}} < 4$ GeV/c (left panel) and $4 < p_{\mathrm{T}}^{\mathrm{h}} < 6$ GeV/c (right panel). The solid horizontal lines represent the assigned systematic.

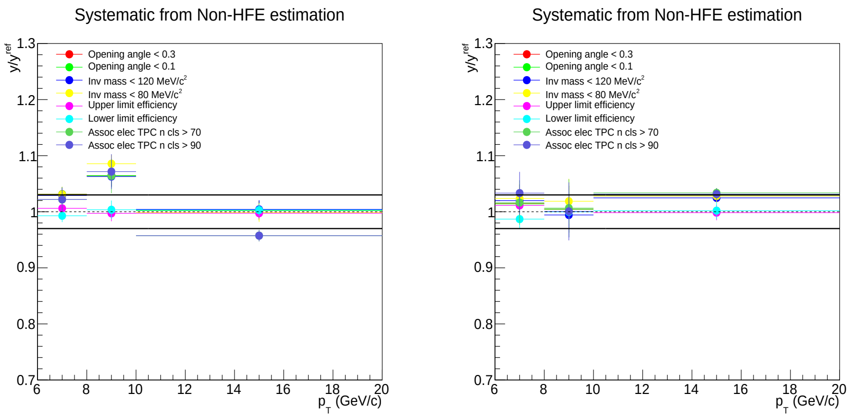

Figure 38: Systematics on the non-heavy flavour electron estimation for $2 < p_{\mathrm{T}}^{\mathrm{h}} < 4$ GeV/c (left panel) and $4 < p_{\mathrm{T}}^{\mathrm{h}} < 6$ GeV/c (right panel). The solid horizontal lines represent the assigned systematic.

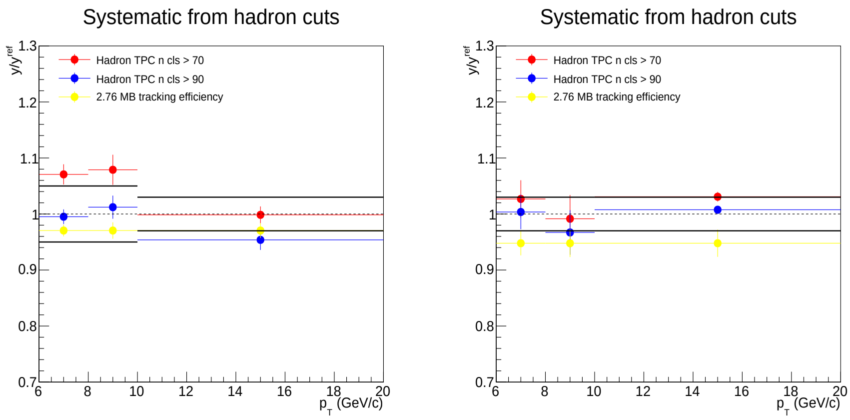

Figure 39: Systematics on the hadrons for $2 < p_{\mathrm{T}}^{\mathrm{h}} < 4$ GeV/c (left panel) and $4 < p_{\mathrm{T}}^{\mathrm{h}} < 6$ GeV/c (right panel). The solid horizontal lines represent the assigned systematic.

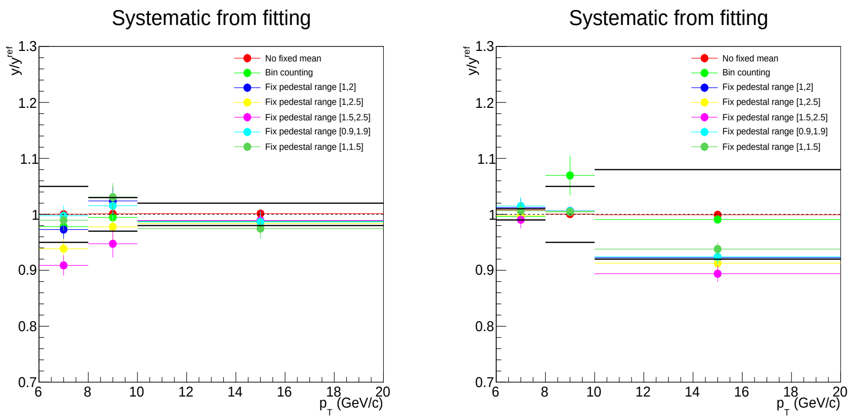

Figure 40: Systematics on the fitting procedure for $2 < p_{\mathrm{T}}^{\mathrm{h}} < 4$ GeV/c (left panel) and $4 < p_{\mathrm{T}}^{\mathrm{h}} < 6$ GeV/c (right panel). The solid horizontal lines represent the assigned systematic.

7.3 Gluon splitting

There are multiple ways to produce heavy quarks. The two most important ones are pair creation and gluon splitting. In order to estimate the dependence of the beauty fraction result on the template, the gluon splitting fraction of the template is varied. This was done by storing the $\Delta\varphi$ distributions from electrons from gluon splitting quarks and non-gluon splitting quarks in the MC sample separately. The event is tagged as a gluon splitting event if the quark has a gluon as mother and if the gluon has another daughter that is the anti-particle of the quark. The templates for electrons from B or D with a gluon splitting

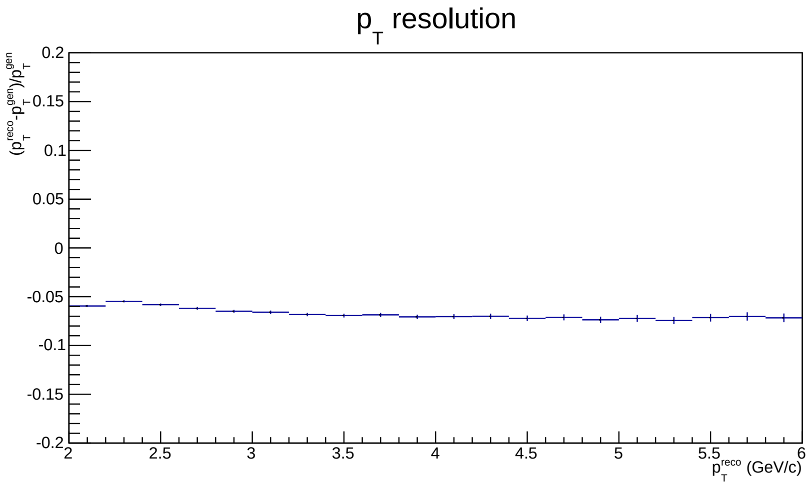

Figure 41: The p_{T} resolution as a function of the reconstructed hadron p_{T}.

fraction f is then defined as:

$$\frac{\mathrm{d}N}{\mathrm{d}\Delta\varphi_{\mathrm{e-h}}} = f\frac{\mathrm{d}N^{\text{gluon splitting}}}{\mathrm{d}\Delta\varphi_{\mathrm{e-h}}} + (1-f)\frac{\mathrm{d}N^{\text{non gluon splitting}}}{\mathrm{d}\Delta\varphi_{\mathrm{e-h}}} \quad . \tag{14}$$

This procedure allows us to change the fraction of gluon splitting for electrons from B and D independently by using different values for f for both templates. The result can be found in Figure 36.

7.4 p_{T} resolution

The measured momentum of a track is not exactly its real momentum. There is a small uncertainty in the measurement. The systematic due to this p_{T} resolution was determined by calculating the relative difference between the reconstructed and generated tracks using the heavy flavour electron enhanced MC sample. This is shown in Figure 41. By fitting $2 < p_{\mathrm{T}}^{\mathrm{h}} < 4$ GeV/c and $4 < p_{\mathrm{T}}^{\mathrm{h}} < 6$ GeV/c with a straight line the values were determined.

7.5 Table of systematic errors

Table 5: Systematics on the relative beauty fraction.

Source	$p_{\mathrm{T}}^{\mathrm{e}}$ (GeV/c): 6-10.5	10.5-18
Electron identification	4%	8%
Non-HFE reconstruction	3%	7%
Hadrons	6%	6%
Fitting	5%	5%
Gluon splitting fraction	4%	4%
Total:	**10%**	**14%**

Table 6: Systematics on the yield.

Source	$2 < p_{\mathrm{T}}^{\mathrm{h}} < 4$ GeV/c			$4 < p_{\mathrm{T}}^{\mathrm{h}} < 6$ GeV/c		
	$p_{\mathrm{T}}^{\mathrm{e}}$ (GeV/c): 6-8	8-10	10-20	6-8	8-10	10-20
Electron identification	4%	4%	4%	7%	7%	7%
Non-HFE reconstruction	3%	3%	3%	3%	3%	3%
Hadrons	5%	5%	3%	3%	3%	3%
Fitting	5%	3%	2%	1%	5%	8%
p_{T} resolution	6%	6%	6%	7%	7%	7%
Total:	**11%**	**10%**	**9%**	**11%**	**11%**	**13%**

8 Results

8.1 Relative beauty contribution

By using the procedure explained in Section 5, the relative beauty fraction is extracted as a function of p_T^e. Figure 42 shows the measured beauty fraction.

Figure 43 shows the measured beauty fraction together with measurements with ALICE using the impact parameter method [12] and the FONLL prediction [5]. The impact parameter method is an independent method from this analysis, where the cross section of $B \to e$ and $D \to e$ are measured. Equation 2 is used to calculate r_B.

Figure 44 shows the measured beauty fraction together with measurements from e-h correlations in pp at $\sqrt{s} = 2.76$ TeV and the FONLL curves for both 7 TeV and 2.76 TeV.

The results are in agreement with the prediction from FONLL calculations, impact parameter measurements from ALICE and the e-h measurements from ALICE at $\sqrt{s} = 2.76$ TeV (paper in preparation) [13].

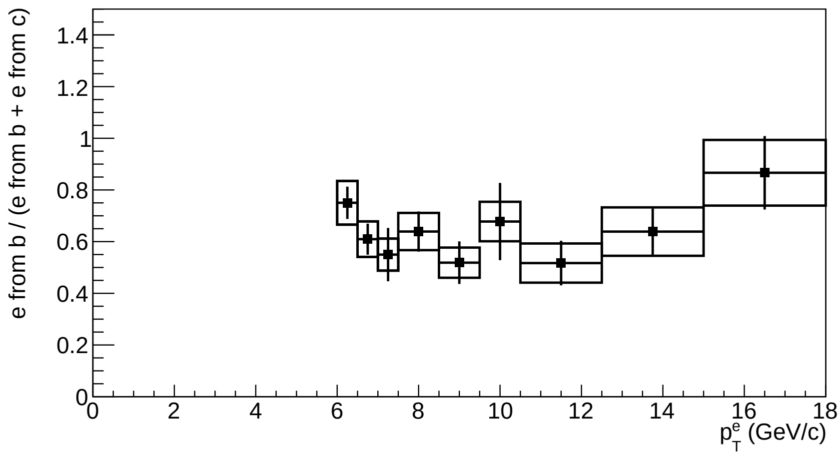

Figure 42: Relative beauty fraction as function of p_T^e for this analysis.

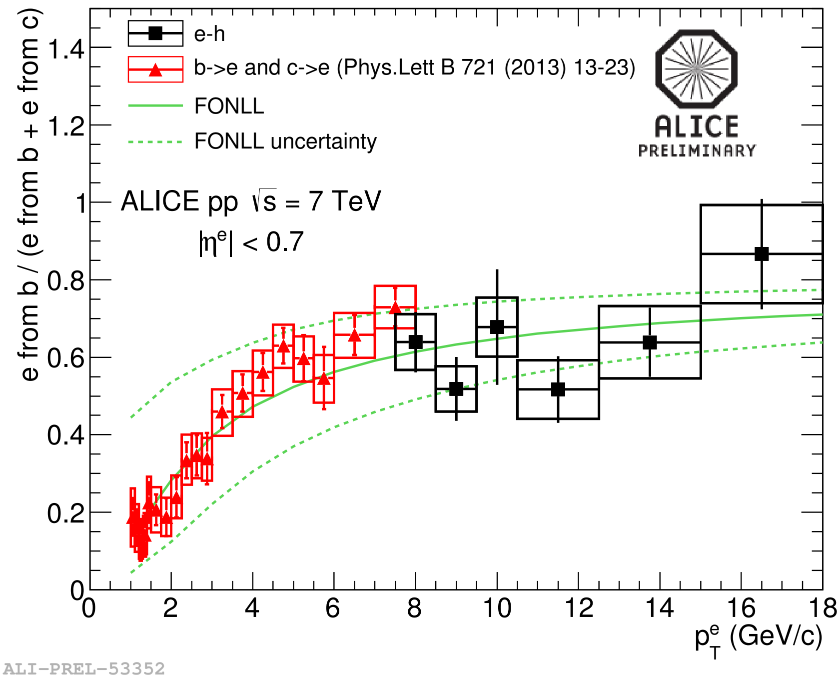

Figure 43: Relative beauty fraction as function of $p_{\mathrm{T}}^{\mathrm{e}}$ for this analysis (black points) and with the impact parameter method (red points). The green solid line is the prediction from FONLL and the green dotted lines are the uncertainty of this calculation.

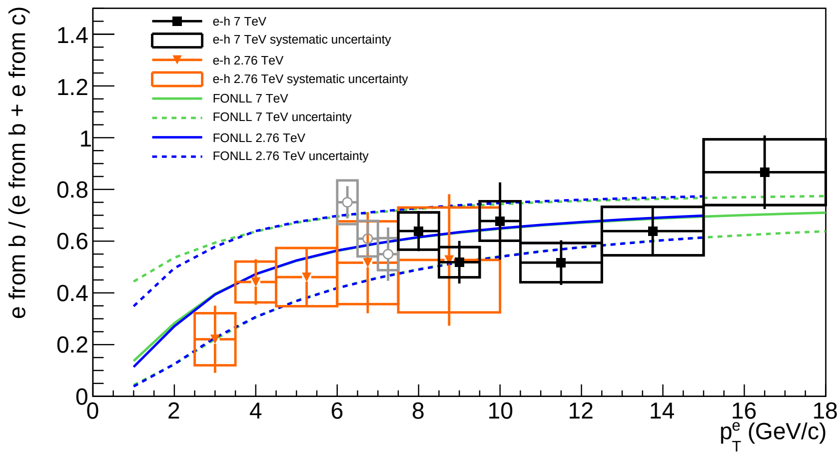

Figure 44: Relative beauty fraction as function of $p_{\mathrm{T}}^{\mathrm{e}}$ for this analysis (black points) and e-h correlation analysis at 2.76 TeV (red points). The green (blue) solid line is the prediction from 7 TeV (2.76 TeV) FONLL and the green (blue) dotted lines are the uncertainty bands of this calculation.

8.2 Baseline measurement

The near-side yield is extracted from the azimuthal angular correlation distribution between heavy flavour electrons and charged hadrons. Figure 45 shows the yield in comparison to the yield from Pb-Pb collisions at $\sqrt{s_{\mathrm{NN}}} = 2.76$ TeV for central (0-8% centrality) [14] and semi-central collisions (20-50%) [15] in the two hadron p_{T} bins.

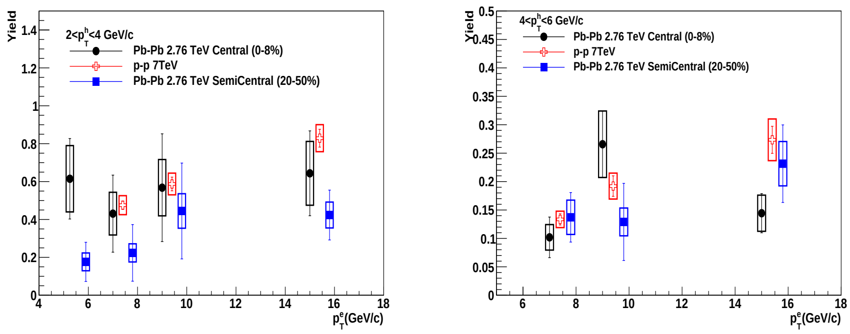

Figure 45: The near-side yield obtained from the fit for the central, semi-central Pb-Pb and pp analysis for $2 < p_{\mathrm{T}}^{\mathrm{h}} < 4$ GeV/c (left panel) and $4 < p_{\mathrm{T}}^{\mathrm{h}} < 6$ GeV/c (right panel) as a function of $p_{\mathrm{T}}^{\mathrm{e}}$.

The ratio of the yield in central Pb-Pb collisions at $\sqrt{s} = 2.76$ TeV to the yield in pp collisions at 7 TeV (referred to as I_{AA}) is as shown in Figure 46. The ratio shows an $I_{\mathrm{AA}} \approx 1$ within statistical and systematic error showing no enhancement or suppression.

The ratio of yield in semi-central Pb-Pb collisions at 2.76 TeV to the yield in pp collisions at 7 TeV is as shown in Figure 47. This ratio is below 1 for the first hadron p_{T} bin and around 1 for the second hadron p_{T} bin.

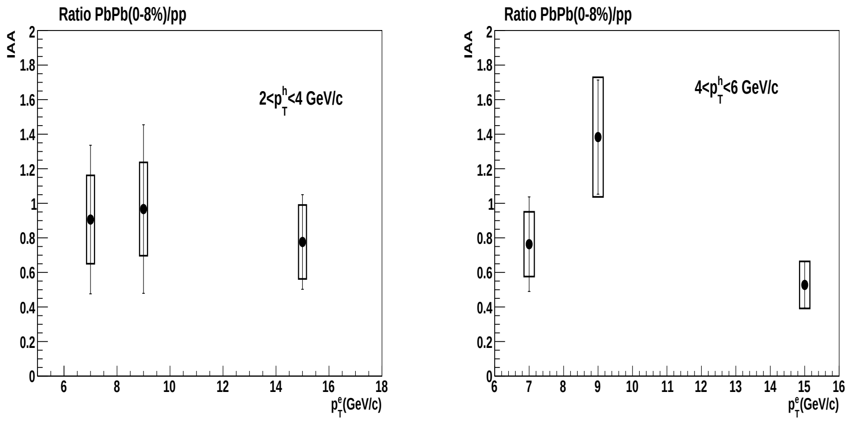

Figure 46: The ratio of yield in central Pb-Pb collisions at 2.76 TeV to the yield in pp collisions at 7 TeV for $2 < p_{\mathrm{T}}^{\mathrm{h}} < 4$ GeV/c (left), $4 < p_{\mathrm{T}}^{\mathrm{h}} < 6$ GeV/c (right) as a function of $p_{\mathrm{T}}^{\mathrm{e}}$.

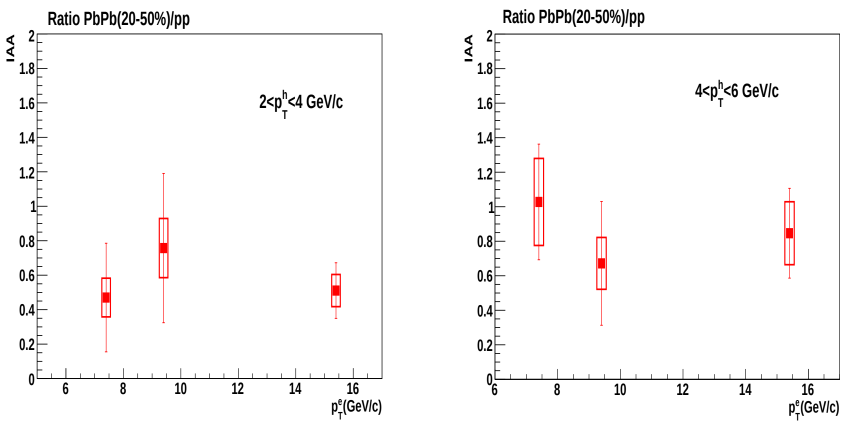

Figure 47: The ratio of yield in semi-central Pb-Pb collisions at 2.76 TeV to the yield in pp collisions at 7 TeV for $2 < p_{\mathrm{T}}^{\mathrm{h}} < 4$ GeV/c (left), $4 < p_{\mathrm{T}}^{\mathrm{h}} < 6$ GeV/c (right) as a function of $p_{\mathrm{T}}^{\mathrm{e}}$.

9 Conclusions

The azimuthal angular correlation between heavy flavour decay electrons and charged hadrons (e-h) were measured in pp collisions at $\sqrt{s} = 7$ TeV.

The relative beauty contribution to the heavy flavour decay electron yield was extracted by fitting the data points with Monte Carlo templates. FONLL calculations are in agreement with the measurement. The measurements from ALICE using the impact parameter method at $\sqrt{s} = 7$ TeV and the e-h correlations at $\sqrt{s} = 2.76$ TeV agree with the measurement presented here. The result has a higher momentum range than shown before. The results now extend to $p_{\mathrm{T}} = 18$ GeV/c, while previously only $p_{\mathrm{T}} = 8$ GeV/c for the IP method was reached and $p_{\mathrm{T}} = 10$ GeV/c for the e-h correlation measurement at lower center-of-mass energy.

In addition, the near-side yield from the correlation function was extracted as a function of $p_{\mathrm{T}}^{\mathrm{e}}$ and used as a baseline for measurements in central and semi-central Pb-Pb collisions in two hadron p_{T} bins of $2 < p_{\mathrm{T}}^{\mathrm{h}} < 4$ GeV/c and $4 < p_{\mathrm{T}}^{\mathrm{h}} < 6$ GeV/c. The I_{AA} shows a value around 1, albeit with large statistic and systematic errors that appear due to the low statistic in Pb-Pb measurements.

The measured I_{AA} is around 1.2 for light mesons. Our measured value from the heavy mesons is different from this. There are many possible reasons for this. One of them is that the suppression factor in Pb-Pb is different for D and B mesons. This changes the relative contribution of electrons from D and B in Pb-Pb compared to pp, which affects the I_{AA} on the near side. It is difficult to draw strong conclusions from the data, since the uncertainties are quite large.

References

[1] ATLAS Collaboration, Phys. Lett. B **716**, 1 (2012).

[2] CMS Collaboration, Phys. Lett. B **716**, 30 (2012).

[3] M. Cacciari et al, JHEP **0103**, 006 (2001).

[4] J. Adams et al, Phys. Rev. Lett. **91**, 072304 (2003).

[5] M. Cacciari et al, JHEP **1210**, 137 (2012).

[6] ALICE Collaboration, Phys. Rev. Lett. **108**, 092301 (2012).

[7] ALICE Collaboration, J. Phys. G: Nucl. Part. Phys. **30**, 1517 (2004).

[8] R. Bellwied, ALICE EMCal Physics Performance Report, arXiv:1008.0413 [physics.ins-det], 2010.

[9] R. Brun and F. Rademakers, Nucl. Inst. & Meth. in Phys. Res. A **389**, 81 (1997).

[10] R. S. de Rooij, Prompt D^{*+} production in proton-proton and lead-lead collisions, measured with the ALICE experiment at the CERN Large Hadron Collider, PhD thesis, Utrecht University, 2013.

[11] H. Bethe and J. Ashkin, Experimental Nuclear Physics (Ed. E. Segré) , 253 (1953).

[12] ALICE Collaboration, Phys. Lett. B **721**, 13 (2013).

[13] Azimuthal angular correlations of heavy flavour decay electrons and charged hadrons in proton-proton collisions at $\sqrt{s} = 2.76$ TeV using the ALICE detector, ALICE analysis note, 2012, `https://aliceinfo.cern.ch/Notes/node/130`.

[14] Study of the azimuthal angular correlations between heavy flavour decay electrons and charged hadrons in lead-lead collisions at $\sqrt{s_{\mathrm{NN}}} = 2.76$ TeV using the ALICE detector, ALICE analysis note, 2013, `https://aliceinfo.cern.ch/Notes/node/200`.

[15] N. Mohammadi, Azimuthal angular correlations between heavy-flavour electrons and charged hadrons in semi-central lead-lead collisions at $\sqrt{s_{\mathrm{NN}}} = 2.76$ TeV at ALICE , Master's thesis, Utrecht University, 2013.